9-15-1992

Lattice Dynamics of Solid C_{60}

Taner Yildirim
University of Pennsylvania, taner@seas.upenn.edu

A. Brooks Harris
University of Pennsylvania, harris@sas.upenn.edu

Lattice Dynamics of Solid C_{60}

Abstract
The lattice dynamics of C_{60} has been studied first by means of group theory and then by diagonalizing the dynamical matrix for two recently proposed intermolecular potentials. The libron and phonon energies are calculated as a function of momentum along various symmetry directions with and without phonon–libron interactions. The effects of these interactions on the density of states are also discussed. Explicit expressions for the energies of these modes at zero wave vector are given. It is found that both potential models have nearly the same phonon but a somewhat different libron spectrum. The calculated libron energies agree reasonably well with currently available experimental results.

Disciplines
Physics | Quantum Physics

Lattice dynamics of solid C_{60}

T. Yildirim and A. B. Harris
Department of Physics, University of Pennsylvania, Philadelphia, Pennsylvania 19104
(Received 16 April 1992)

The lattice dynamics of C_{60} has been studied first by means of group theory and then by diagonalizing the dynamical matrix for two recently proposed intermolecular potentials. The libron and phonon energies are calculated as a function of momentum along various symmetry directions with and without phonon–libron interactions. The effects of these interactions on the density of states are also discussed. Explicit expressions for the energies of these modes at zero wave vector are given. It is found that both potential models have nearly the same phonon but a somewhat different libron spectrum. The calculated libron energies agree reasonably well with currently available experimental results.

I. INTRODUCTION

Recently it has been established that C_{60} molecules in solid C_{60} undergo an orientational ordering transition at a temperature T_c of about 250 K.[1] For temperature $T > T_c$ the molecular orientations are uncorrelated over distances of more than a few lattice constants.[2] In this phase the molecular centers form an fcc Bravais lattice with space group $Fm\bar{3}m$ (Ref. 3) and the molecules are freely rotating.[4] For $T < T_c$ an orientationally ordered structure is formed with four molecules per unit cell.[1] It has been shown[5] that there are only three possible space groups for completely oriented icosahedra centered on fcc lattice positions such that there are four molecules per unit cell. It has been established[6,7] that the ordered structure is that of the space group $Pa3$ (T_h^6). In this structure the center of gravity of each molecule remains on its fcc lattice position. This structure may be viewed as consisting of four interpenetrating simple cubic sublattices, on each of which molecules assume a given fixed orientation as shown schematically in Fig. 1. For each sublattice this orientation is obtained by rotation about the local threefold axis through a setting angle $\phi \sim 24°$ from an initial *standard* orientation in which twofold axes are aligned along [100] directions. One choice of the local threefold axes is listed in Table I. Although the $Pa3$ space group has no fourfold rotation or fourfold screw axes, cubic symmetry is attained by screw axes which result in the different [111] directions being equivalent. Since there is long-range orientational order, we know that there will be elementary orientational excitations, called librons, which describe orientational properties near the orientational ground state and which are the focus of the present paper.

TABLE I. Molecular positions and threefold axes of symmetry for sites in the unit cell. Here $\mathbf{X}(\mu)$ is the position of the center of mass of the molecule μ in the unit cell and a is the simple-cubic lattice constant.

μ	$\mathbf{X}(\mu)$	Local threefold axis
1	$(0,0,0)a$	[111]
2	$(\frac{1}{2},0,\frac{1}{2})a$	$[\bar{1}\bar{1}1]$
3	$(0,\frac{1}{2},\frac{1}{2})a$	$[\bar{1}1\bar{1}]$
4	$(\frac{1}{2},\frac{1}{2},0)a$	$[1\bar{1}\bar{1}]$

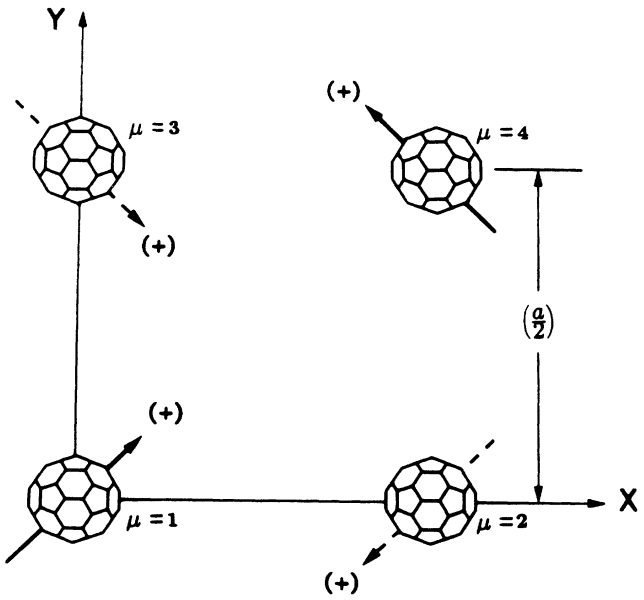

FIG. 1. The crystal structure of solid C_{60} ($Pa3$) (Refs. 5–7). For each molecule, the arrows indicate which of the crystal [111] directions corresponds to the local threefold axes as listed in Table I. Molecules with solid arrows are in the $z = 0$ plane and those with dashed arrows are in the plane $z = \frac{1}{2}a$. The end of the arrow labeled (+) points out of the page. To get the equilibrium orientational configuration, each molecule must be rotated from its standard orientation through the setting angle, Φ, about the local axes indicated by arrows. Values of Φ are given in Refs. 27 and 6 as 22° and 26°, respectively. The orientations of the single and double bonds are represented as they would appear *before* rotation through the setting angle Φ.

Although we will be concerned with C_{60} in its $Pa3$ phase, we should note that the structure and phase diagram of pure solid C_{60} is still controversial. Very recently, there have been suggestions of further phase transitions in pure C_{60} at temperatures below 250 K. For instance, evidence has been obtained for a glass transition at about 90 K.[8] There is currently much debate as to whether or not this is a true phase transition as contrasted to a gradual evolution in dynamics which one would see when the experimental time scales become comparable to the relaxation time. However, a transition such as this does not necessarily indicate that the $Pa3$ structure becomes unstable at low temperature. A possible transition which would have greater relevance for the calculations of the present paper is that suggested by the electron diffraction and microscopy study of Tendeloo *et al.*[9] They interpret their experimental data as showing a doubling of the unit cell parameter along all three [100] directions. The structure they propose is one in which molecules separated by a displacement a along each [100] direction are alternately rotated by angles $+\phi$ and $-\phi$. This suggestion seems implausible to us. An alternative structure of this type would be one in which each molecule is rotated by a small displacement angle $\delta\phi$ relative to their equilibrium positions in the usual $Pa3$ structure. A distorted structure of this type would give rise to additional Bragg reflections (not yet seen in other experiments) and would also give rise to anomalies in the libron spectrum. Since the structure is not yet confirmed by several experiments, we do not consider it here.

A calculation of the libron spectrum requires an orientational potential which is consistent with the $Pa3$ ground state. By now two such potentials have been proposed.[10,11] Li *et al.*[12] have given libron spectra from their potential, and our results confirm theirs. Here we calculate the libron and phonon spectrum from the potential proposed by Sprick, Cheng, and Klein[11] in order to compare results from the two potentials. These calculations can be carried out in a standard formalism reviewed by Ref. 13, for instance. An appropriate way to carry out these calculations is to assume that deformations of the molecule require much more energy than the elementary excitations due to intermolecular translations or rotations.[14] Since there are four molecules per simple cubic unit cell, we expect to have $4\times 6 = 24$ modes in the phonon–libron spectrum. If we neglect coupling between librons and phonons, each of these degrees of freedom will have 12 modes for each allowed wave vector.

It is useful to recall the results for other systems having the same crystal structure, $Pa3$. In particular, many of the diatomic molecular solids have this structure, including those of N_2,[15] CO,[16] and H_2.[17,18] The main difference in the case of diatomics is that each diatomic molecule has only two angular coordinates, whereas the rigid body C_{60} has three such coordinates. We will show below a dispersion relation for librons in solid H_2.[19] This calculation shows that the dispersion in the libron band is smaller than or comparable to the average libron energy. In other words, librons are well approximated by neglecting completely their dispersion, in which case they are so-called Einstein modes. Of course, in experiments where a quantity similar to the libron density of states is observed, such an approximation should not be used. The complete libron–phonon excitation spectrum calculated by Mertens and Biem[20] for solid H_2 shows that the libron–phonon coupling is quite small.[21,22] As we shall see, the libron spectrum for C_{60} is quite similar to that for solid H_2 even though the physics behind the orientational interactions is quite different in the two cases. Seemingly the constraints of group theory are quite severe.

Here we calculate only a few of the properties which depend on the libron and phonon frequencies. As we have mentioned, our results for the libron and phonon dispersion relations and density of states do reproduce the results of Li *et al.*[12] for their potential. Concerning the elastic constants we do have a minor discrepancy possibly caused by some confusion concerning the scale of wave vectors. Also, we give mean square amplitudes of vibration and rotation, which show that quantum zero-point motion is indeed very small. Using a Lindemann criterion, we estimate the melting temperature to be of order 1700 K. However, such a criterion may not be definitive for such a large molecule. Our results also include the symmetry of the libron and phonon modes. This information, not given by Li *et al.*, could presumably help in the identification of modes as potentially observable via inelastic neutron scattering. The quantities we calculate will facilitate an experimental test of the potentials heretofore proposed and will therefore be helpful in further refinements of these potentials.

Briefly this paper is organized as follows. In Sec. II we review the formalism to be used in our calculations. The group theoretical analysis is outlined in Sec. III, but most of the details are given in Appendixes A and B. For instance, in Appendix B we give the block-diagonal form of the dynamical matrix at zero wave vector. This form could easily be used to obtain libron frequencies at zero wave vector for other orientational potentials. Section IV contains our results. Here we show dispersion curves and density of states for both potential models. We give results both with and without the inclusion of libron–phonon interactions. We tabulate the elastic constants implied by our lattice-dynamical calculations. Here we also give a brief discussion of the implications our results have for optical and scattering properties. In Sec. V we estimate the amplitude of thermally excited translational and orientational excitations. We then employ a Lindemann criterion to estimate the melting temperature of C_{60}. Our conclusions are summarized in Sec. VI.

II. LATTICE DYNAMICS

In this section we discuss the calculation of the libron and phonon dispersion relations within the harmonic approximation for perfectly rigid C_{60} molecules. We first give the generalized coordinates needed to discuss the orientational and translational excitations out of the ground state. We then use these coordinates to form the dynamical matrix from which the normal modes of small oscillations are obtained. Next we discuss the conditions for equilibrium. These conditions provide the relation be-

tween the lattice constant and the setting angle of the molecule and parameters used in the intermolecular potential. Finally, we describe the recently proposed intermolecular potentials for which we carry out calculations.

A. Generalized coordinates

The coordinate basis used in the present work is now described. To implement the rigid-body approximation mentioned above, we introduce a set of molecule-fixed coordinates, whose origin is at the center of gravity of the molecule. In this set of coordinates the atoms are located at positions $\mathbf{x}(k)$ for $k = 1, 2, ..., 60$. We may then express the α component of the position of the kth atom of the μth molecule in unit cell a as

$$X_\alpha(a,\mu,k) = \bar{X}_\alpha(a,\mu) + t_\alpha(a,\mu) + \sum_\rho \Gamma^\mu_{\alpha\rho} x_\rho(k), \quad (1)$$

where $\bar{X}_\alpha(a,\mu)$ denotes the equilibrium position of the center of mass of the μth molecule in cell a (see Table I) and $x_\rho(k)$ is the ρth component of the position of the kth atom in the molecule-fixed coordinate system. Here $\mathbf{\Gamma}^\mu$ is the rotation matrix whose elements $\Gamma^\mu_{\alpha\rho}$ give the direction cosine between the crystal-fixed α axis and the molecule-fixed axis ρ. Also, $t_\alpha(a,\mu)$ is the α component of the translational displacement of the center of mass of the μth molecule in unit cell a. Since we shall treat the translational and rotational motions along with their coupling in the same framework it is convenient to define three translational coordinates as mass-weighted displacements of the center of mass along the three directions of the Cartesian axes by the relation

$$u^t_\rho(a,\mu) = (M)^{1/2} t_\rho(a,\mu), \quad (2)$$

where $M = 1.2 \times 10^{-24}$ kg is the mass of C_{60}.

For the three degrees of rotational freedom, we define three rotational coordinates as inertia moment-weighted rotations around the three molecular axes

$$u^r_\rho(a,\mu) = (I)^{1/2} \theta_\rho(a,\mu), \quad (3)$$

where $I = 1 \times 10^{-43}$ kg m^2 is the moment of inertia of C_{60}. The relation between the crystal-fixed Cartesian coordinates and the rotations $\theta_\rho(a\mu)$ can be obtained from Eq. (1) once the dependence of the direction cosines $\Gamma^\mu_{\alpha\rho}$ on the rotations $\theta_\rho(a,\mu)$ is specified,[23,24]

$$\Gamma^\mu_{\alpha\rho} = \Lambda^\mu_{\alpha\rho} + \sum_{\sigma\tau} \Lambda^\mu_{\alpha\tau} \epsilon_{\tau\rho\sigma} \theta_\sigma(a,\mu) - \frac{1}{2} \sum_{\tau\omega} \sum_{\sigma\chi} \Lambda^\mu_{\alpha\tau} \epsilon_{\tau\omega\sigma} \epsilon_{\rho\omega\chi} \theta_\sigma(a,\mu) \theta_\chi(a,\mu), \quad (4)$$

where $\Lambda^\mu_{\alpha\rho}$ is the equilibrium value of $\Gamma^\mu_{\alpha\rho}$. The infinitesimal rotation $\theta_\rho(a,\mu)$ is taken about the molecule-fixed ρ axis. $\epsilon_{\tau\rho\sigma}$ takes the value zero unless all three indices are different. It is equal to 1 if the indices are in the cyclic order xyz and -1 for the order zyx.

B. Dynamical matrix

The analysis of the vibrational dynamics of a crystal by diagonalizing the dynamical interaction matrix is to be found in almost all solid-state physics texts[13] and will be very briefly paraphrased here merely to establish a convenient notation.

After expanding the potential energy of a molecular crystal in terms of $\mathbf{u}^t(a,\mu)$ and $\mathbf{u}^r(a,\mu)$, writing down the equations of motion (in the harmonic approximation), and taking advantage of the translational symmetry by the following Fourier transform:

$$u^i_\alpha(\mathbf{q},\mu) = \frac{1}{\sqrt{N}} \sum_a u^i_\alpha(a,\mu) e^{-i\mathbf{q}\cdot\mathbf{X}(a)}, \quad i = t, r, \quad (5)$$

where N is the number of unit cells, we get the following system of equations determining the normal modes and frequencies of the system:

$$\omega^2 u^t_\alpha(\mathbf{q},\mu) = \sum_{\beta,\nu} \{ D^{tt}_{\alpha\beta}(\mathbf{q};\mu\nu) u^t_\beta(\mathbf{q},\nu) + D^{tr}_{\alpha\beta}(\mathbf{q};\mu\nu) u^r_\beta(\mathbf{q},\nu) \}, \quad (6)$$

$$\omega^2 u^r_\alpha(\mathbf{q},\mu) = \sum_{\beta,\nu} \{ D^{rt}_{\alpha\beta}(\mathbf{q};\mu\nu) u^t_\beta(\mathbf{q},\nu) + D^{rr}_{\alpha\beta}(\mathbf{q};\mu\nu) u^r_\beta(\mathbf{q},\nu) \}. \quad (7)$$

Here

$$D^{ii'}_{\alpha\beta}(\mathbf{q};\mu\nu) = \frac{1}{\sqrt{m^i m^{i'}}} \sum_b V^{ii'}_{\alpha\beta}(o\mu;b\nu) e^{i\mathbf{q}\cdot\mathbf{X}(b)}, \quad i, i' = t, r, \quad (8)$$

where $m^i = M, I$ for $i = t, r$, respectively, and the $V^{ii'}_{\alpha\beta}(o\mu;b\nu)$ is the force constant given by

$$V^{ii'}_{\alpha\beta}(o\mu;b\nu) = \left(\frac{\partial^2 V_I}{\partial u^i_\alpha(o,\mu) \partial u^{i'}_\beta(b,\nu)} \right)_o, \quad i, i' = t, r, \quad (9)$$

where V_I is the interaction potential and $(\cdots)_o$ signifies that the derivatives are to be evaluated with all molecules in their respective equilibrium positions and orientations.

We may write Eqs. (6) and (7) in the following matrix form:

$$\mathbf{D}(\mathbf{q})\mathbf{U}(\mathbf{q}) = \omega^2 \mathbf{U}(\mathbf{q}), \quad (10)$$

where $\mathbf{D}(\mathbf{q})$ is the 24×24 dynamical matrix

$$\mathbf{D}(\mathbf{q}) = \begin{pmatrix} D^{tt}(\mathbf{q}) & D^{tr}(\mathbf{q}) \\ D^{rt}(\mathbf{q}) & D^{rr}(\mathbf{q}) \end{pmatrix}, \quad (11)$$

and $\mathbf{U}(\mathbf{q}) = (\mathbf{u}^t(\mathbf{q},1), \ldots, \mathbf{u}^t(\mathbf{q},4), \mathbf{u}^r(\mathbf{q},1), \ldots, \mathbf{u}^r(\mathbf{q},4))$ with $\mathbf{u}^i(\mathbf{q},\mu) = (u^i_x(\mathbf{q},\mu), u^i_y(\mathbf{q},\mu), u^i_z(\mathbf{q},\mu))$ are the eigenvectors.

For the construction of the dynamical matrix elements given in Eq. (8) we need to specify the form of the crystal potential. Neglecting multimolecule interactions, the in-

termolecular potential may be expressed as the sum over all pairwise interaction between molecules

$$V_I = \frac{1}{2}\sum_{a\mu}\sum_{b\nu}\Phi(a\mu;b\nu), \tag{12}$$

where $\Phi(a\mu;a\mu)=0$.

It is convenient to express the dynamical matrix in Eq. (8) as a sum of diagonal and off-diagonal parts in sublattice indices μ and ν. Namely from Eqs. (8) and (12) one gets

$$D^{ii'}_{\alpha\beta}(\mathbf{q};\mu\nu) = \frac{1}{2}\sum_{b}\sum_{\lambda}\left\{\left(\frac{\partial^2\Phi(o\mu,b\lambda)}{\partial u^i_\alpha(o,\mu)\partial u^{i'}_\beta(o,\mu)}\right)_o\delta_{\mu,\nu}+\left(\frac{\partial^2\Phi(o\mu,b\lambda)}{\partial u^i_\alpha(o,\mu)\partial u^{i'}_\beta(b,\lambda)}\right)_o\delta_{\lambda,\nu}e^{-i\mathbf{q}\cdot\mathbf{X}(b)}\right\}. \tag{13}$$

The explicit expressions for the force constants

$$\left(\frac{\partial^2\Phi(o\mu,b\lambda)}{\partial u^i_\alpha(o,\mu)\partial u^{i'}_\beta(o,\mu)}\right)_o \quad\text{and}\quad \left(\frac{\partial^2\Phi(o\mu,b\lambda)}{\partial u^i_\alpha(o,\mu)\partial u^{i'}_\beta(b,\lambda)}\right)_o$$

can be found in Ref. 25.

After having introduced the *harmonic approximation*, it is important to establish the form of the total equilibrium conditions. These equations provide the relation between the lattice constant and setting angle of the molecule and parameters used in the intermolecular potential.

For total equilibrium we have to satisfy both force- and stress-free conditions which are, respectively, given by

$$\sum_{b\nu}\left(\frac{\partial\Phi(o\mu,b\nu)}{\partial u^i_\alpha(o,\mu)}\right)_o = 0,$$

$$i=t,r,\quad \alpha=x,y,z,\quad \mu=1,2,3,4 \tag{14}$$

and

$$\sum_{b\mu\nu}\left\{\left(\frac{\partial\Phi(o\mu,b\nu)}{\partial u^t_\sigma(b,\nu)}\right)_o R_\tau(o\mu,b\nu)+\left(\frac{\partial\Phi(o\mu,b\nu)}{\partial u^t_\tau(b,\nu)}\right)_o R_\sigma(o\mu,b\nu)\right\}=0,\quad \tau,\sigma=x,y,z, \tag{15}$$

where $R_\tau(o\mu,b\nu)=u^t_\tau(b,\nu)-u^t_\tau(o,\mu)$. Since there are four molecules in the unit cell, the force-free condition gives 24 conditions while the stress-free condition gives 6. However, the number of these conditions is considerably reduced by the symmetry of the crystal.

From group theory we know that *molecules which are interchangeable by rotations (proper or improper) together form a crystallographically distinct species and if one of the member is force free all are force free.* Since orientationally ordered C_{60} forms a simple cubic system with four symmetry-related molecules in the unit cell, the number of independent force-free conditions is reduced to 6. A further reduction in this number is a consequence of the site symmetry $S_6(\bar{3})$. According to Eq. (14) the gradient of the potential must vanish at equilibrium. This condition will be satisfied if the gradient involving coordinates which are invariant under the site symmetry operations vanishes. The only such invariant (totally symmetric) coordinate is the uniform rotation of all molecules about their local threefold axis. Thus the force-free condition is simply

$$\left(\frac{\partial V_I}{\partial\phi}\right)_{\phi=\phi_o}=0, \tag{16}$$

where ϕ is the setting angle whose equilibrium value is ϕ_0. Note that for solids of linear molecules, such as solid H_2 (Refs. 17 and 18) or N_2 or CO (Refs. 15 and 16) (which crystallize with the same space group, $Pa3$, as C_{60}), rotation about the linear axis is meaningless. Thus in these systems there is no such ϕ coordinate and consequently there is no condition analogous to Eq. (16)

The stress-free condition fixes the equilibrium shape of the unit cell. A discussion similar to that for the force-free case shows that for cubic symmetry there is only one symmetric deformation of the unit cell. *The cube can only be uniformly expanded.* As a result there is only one independent stress-free condition,

$$\left(\frac{\partial V_I}{\partial a}\right)_{a=a_o}=0. \tag{17}$$

In summary, for C_{60} in the $Pa3$ structure, we have two independent conditions for equilibrium given in Eqs. (16) and (17). Thus there are two constraints on the parameters in the potential.

C. Intermolecular potential model

We now discuss models for the intermolecular potential Φ in Eq. (12) for which we perform calculations. Recently two different potentials to describe the interactions between C_{60} molecules have been proposed.[10,11] In both cases, the part of the intermolecular potential independent of the molecular orientation is contained in a *Lennard-Jones* (12-6) atom-atom potential. The dependence of the Lennard-Jones potential on orientation is weak and it also predicts[26] that the cubic structure is unstable relative to a tetragonal distortion, contrary to experiment. To remedy this defect, it is necessary to use a more realistic orientational potential. In particular, it has recently been realized that it is important to take proper account of the charge density. In the two models proposed, allowance is made for enhanced electron density in the double bonds relative to that in the single bonds, as we will see in a moment.

The potential proposed in Ref. 10 (denoted potential I) is modeled by introducing effective charges q and $-2q$ ($q=0.27e$) located on the centers of the single and double bonds, respectively. Thus the total interaction between two molecules is

$$\Phi(a\mu,b\nu)=\sum_{k\epsilon a\mu}\sum_{k'\epsilon b\nu}4\epsilon\left\{\left(\frac{\sigma}{R_{kk'}}\right)^{12}-\left(\frac{\sigma}{R_{kk'}}\right)^{6}\right\}+\sum_{m\epsilon a\mu}\sum_{n\epsilon b\nu}\frac{q_m q_n}{R_{mn}},\tag{18}$$

where $R_{kk'}$ (R_{mn}) is the distance between kth C atom (mth bond center) of the molecule $a\mu$ and k'th C atom (nth bond center) of the molecule $b\nu$ and q_m is the effective charge of bond m. The parameters ϵ and σ are taken to be $\epsilon = 2.964$ meV and $\sigma = 3.407$ Å.

In Ref. 11 the intermolecular potential (denoted potential II) is modeled by the interacting bond model in which the 60 atomic 12-6 C sites are supplemented with 30 similar 12-6 D sites located at the centers of double bonds. Furthermore, the stability of $Pa3$ structure is enhanced by assigning a negative bond charge q_D ($q_D = -0.35e$) to the D sites and a compensating positive charge $q_C = -\frac{q_D}{2}$ to the C atoms. The explicit expression for the potential energy between molecules $a\mu$ and $b\nu$ is

$$\Phi(a\mu,b\nu)=\sum_{k\epsilon C}\sum_{k'\epsilon C}4\epsilon\left\{\left(\frac{\sigma_{CC}}{R_{kk'}}\right)^{12}-\left(\frac{\sigma_{CC}}{R_{kk'}}\right)^{6}\right\}+\sum_{k\neq k'\epsilon C,D}4\epsilon\left\{\left(\frac{\sigma_{CD}}{R_{kk'}}\right)^{12}-\left(\frac{\sigma_{CD}}{R_{kk'}}\right)^{6}\right\}+\sum_{k\epsilon D}\sum_{k'\epsilon D}4\epsilon\left\{\left(\frac{\sigma_{DD}}{R_{kk'}}\right)^{12}-\left(\frac{\sigma_{DD}}{R_{kk'}}\right)^{6}\right\}+\sum_{k,k'\epsilon C,D}\frac{q_k q_{k'}}{R_{mn}},\tag{19}$$

where k (k') runs over the C and D sites of the molecule $a\mu$ ($b\nu$). Here $R_{kk'}$ is the distance between sites k and k' and q_k are the effective charges at the centers of the bonds and on the C atoms for $k = D$, C, respectively. The values of the parameters $\epsilon, \sigma_{CC}, \sigma_{CD}$, and σ_{DD} are 1.293 meV, 3.4 Å, 3.5 Å, and 3.6 Å, respectively.

A detailed study of potential I is given in Ref. 10 and is not repeated here. Figure 2(a) shows the variation of potential II with setting angle ϕ. The potential energy has an absolute minimum at $\phi = 25.36°$ which is in good agreement with the experimental values 22° (Ref. 27) and 26°.[6] Figures 2(a) and 2(b) show the potential II as a function of angular displacement of the molecule located at (0,0,0) away from its equilibrium configuration for various rotational axes. Note that there are many local minima which are separated by a potential barrier of height about 150 meV. This value is half of that of potential I in Ref. 10 indicating that it would give a lower glassy transition temperature T_g than the one given in Ref. 10.

III. GROUP THEORETICAL ANALYSIS OF C_{60}

Before we discuss our numerical results obtained from two potential models introduced above, we shall present the group theoretical analysis of the C_{60} crystal. Since the available experimental data are not enough to test

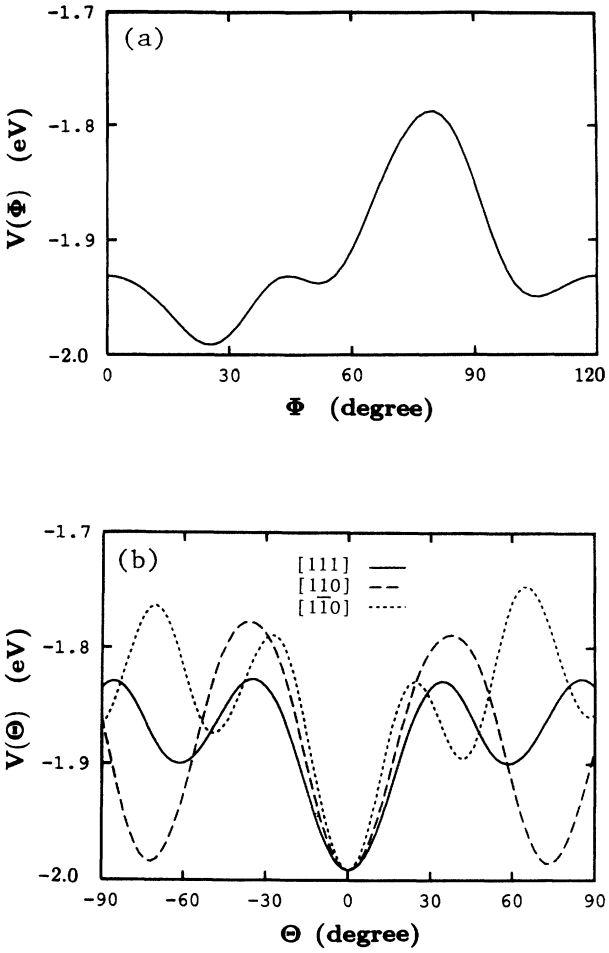

FIG. 2. (a) Top: Variation of the crystal potential energy with setting angle Φ according to potential II. (Molecules in each sublattice are rotated about their [111] directions.) The potential energy has an absolute minimum at $\Phi_o = 25.36°$. (b) Bottom: The potential energy for a C_{60} molecule located at (0,0,0) obtained from potential II as a function of rotation angle away from its equilibrium orientation. [Here only the molecule at (0,0,0) is rotated.] The curves denoted by solid line, long-dashed line, and short-dashed line correspond, respectively, to rotations about [111], [110], and [1$\bar{1}$0] axes of the crystal.

the present potential models the results from group theory which are independent of the force model of the crystal, are most valuable, especially for the analysis of the infrared, Raman, and neutron scattering of the crystals.

From group theory[13,28] one can predict the degeneracy of normal modes for any $\mathbf{q}$ vector in the Brillouin zone. One classifies the normal modes according to the transformation properties of their polarization vectors with respect to symmetry operations, and hence determines the polarization vector of the normal mode when it is given by the symmetry alone. Finally, group theory facilitates the factorization of the dynamical matrix. This requires first the construction of the set of unitary matrices

$$S(\mathbf{q};R)=\begin{pmatrix}T(\mathbf{q};R) & 0\\ 0 & T(\mathbf{q};R)\det(R)\end{pmatrix},\tag{20}$$

where

$$T(\mathbf{q};R)=\begin{pmatrix}\Lambda(1,1)R\cdots\Lambda(1,4)R\\ \vdots\qquad\qquad\vdots\\ \Lambda(4,1)R\cdots\Lambda(4,4)R\end{pmatrix} \tag{21}$$

with

$$\Lambda(\mu,\nu)=\delta(\mu,F(\nu,R))\,e^{i\mathbf{q}\cdot[\mathbf{X}(\mu)-\mathbf{R}\mathbf{X}(\nu)]}. \tag{22}$$

Here R are 3×3 rotational matrices which are elements of the *group of wave vector* $\mathbf{q}$, $\mathbf{G}(\mathbf{q})$. The quantity $\delta(\mu,F(\nu,R))$ describes interchanges in the sublattices, if any. It is a Kronecker delta, and vanishes unless μ corresponds to the sublattice ν via R, in which case it is equal to unity.

In Eq. (20) we used the fact that the transformation properties of both translational and rotational coordinates are the same except that $u^r_\alpha(\mathbf{q},\mu)$ transforms like the component of an axial vector. Note that $\det(R)=\pm1$ for proper and improper rotations, respectively. Therefore, the transformation matrix for $u^r_\alpha(\mathbf{q},\mu)$ differs from that for $u^t_\alpha(\mathbf{q},\mu)$ by inclusion of the factor $\det(R)$. Further, because $u^t_\alpha(\mathbf{q},\mu)$ and $u^r_\alpha(\mathbf{q},\mu)$ transform independently of each other, the off-diagonal parts of $S(\mathbf{q};R)$ in Eq. (20) are zero.

The matrix $S(\mathbf{q};R)$ commutes with the dynamical matrix $D(\mathbf{q})$ given in Eq. (11) for all R in $\mathbf{G}(\mathbf{q})$ and thus the set of matrices $\mathbf{S}(\mathbf{q})=\{\mathbf{S}(\mathbf{q};\mathbf{R})\mid\mathbf{R}\in\mathbf{G}(\mathbf{q})\}$ furnish a *24-dimensional reducible representation* of $\mathbf{G}(\mathbf{q})$. In order to obtain all information about the normal modes mentioned above, one resorts to the familiar reduction formula

$$c_s=\frac{1}{h}\sum_{R\epsilon\mathbf{G}(\mathbf{q})}\chi^{(s)}(\mathbf{q};R)^*\chi(\mathbf{q};R), \tag{23}$$

where

$$\chi^{(s)}(\mathbf{q};R)=\mathrm{Tr}[\tau^{(s)}(\mathbf{q};R)], \tag{24}$$

$$\chi(\mathbf{q};R)=\mathrm{Tr}[S(\mathbf{q};R)], \tag{25}$$

and h is the order of $\mathbf{G}(\mathbf{q})$. The quantity c_s above is the number of times the *irreducible representation* (IR) $\tau^{(s)}(\mathbf{q})$ of dimensionality f_s occurs in the 24-dimensional reducible representation of $S(\mathbf{q})$. Correspondingly, there will be c_s eigenvalues $\omega^2_{s,1}(\mathbf{q}),\omega^2_{s,2}(\mathbf{q}),\ldots,\omega^2_{s,c_s}(\mathbf{q})$ each of which will be f_s-fold degenerate.

After having reviewed the standard group theoretical procedure, we shall now present the results of the group theoretical analysis of lattice vibrations of the solid C_{60}.

C_{60} molecules crystallizes in the simple cubic system, space group T^6_h $(Pa3)$ with four molecules per unit lying on sites of $S_6(3)$ symmetry (Fig. 1). The positions of the four atoms in a primative unit cell are given in Table I. The symmetry elements that will be important are those of the space group which leave the unit cell invariant, in this case $\mathbf{T_h}=\mathbf{i}\times\mathbf{T}$. There are eight threefold rotations $C^{\pm}_{3\mu}$ (μ=1–4) along the appropriate [111] axis, three twofold screw axes $C_{2\alpha}$ ($\alpha=x,y,z$) parallel to the cubic axes. The direct product with the inversion operator $\mathbf{i}$ yields eight $S^{\pm}_{6\mu}$ and three glide planes σ_α. These 24 rotational elements with their corresponding $V(R)$ (*fractional translation*) are given in the 3×3 matrix form in Appendix A. The effect of these rotational elements on the sublattices and Cartesian components, required for the present work, are given in Table II.

The BZ of a simple cubic lattice, showing the high-symmetry points pertinent to the present calculations, is shown in Fig. 3. The 10 special wave vectors of high symmetry in the BZ of simple cubic lattice and elements of T_h that leave these vectors fixed or change by a vector of the reciprocal lattice are given in Table III.

Since Γ $(\mathbf{q}=0)$ is the most important point for many aspects, we provide a detailed group theoretical study of the lattice modes at this point in Appendix B. Particularly, we first find the 24 symmetry-adapted vectors and then after simplifying the dynamical matrix we calculated the energies of libron and phonon modes explicitly in terms of any given potential model. Such information is useful for testing new potentials and for analysis of infrared, Raman, and neutron scattering of the crystal. For other high-symmetry points and lines in BZ our group theoretical analysis is collected in Table IV in the following manner. The first column lists the high-symmetry points and their coordinates in the BZ

TABLE II. Effect of symmetry operations of cubic group $\mathbf{T}$ on molecules and on Cartesian components. The first four rows (i=1–4) shows how sublattice i transforms under the symmetry operation of each column. The last three rows show the effect of each symmetry operation on Cartesian coordinates x, y, and z, when fractional translations are omitted. The screw operations $C_{2\alpha}$ ($\alpha=x,y,z$) are chosen so that $C_{2x}=C_2[100]+(1,1,0)\frac{a}{2}$, $C_{2y}=C_2[010]+(0,1,1)\frac{a}{2}$, and $C_{2z}=C_2[001]+(1,0,1)\frac{a}{2}$, where $C_2[\mathbf{R}]$ is 180° rotation operator about axis $\mathbf{R}$.

E	C_{2x}	C_{2y}	C_{2z}	C^+_{31}	C^+_{32}	C^+_{33}	C^+_{34}	C^-_{31}	C^-_{32}	C^-_{33}	C^-_{34}
1	4	3	2	1	3	4	2	1	4	2	3
2	3	4	1	4	2	1	3	3	2	4	1
3	2	1	4	2	4	3	1	4	1	3	2
4	1	2	3	3	1	2	4	2	3	1	4
x	x	$\bar{x}$	$\bar{x}$	z	$\bar{z}$	z	$\bar{z}$	y	y	$\bar{y}$	$\bar{y}$
y	$\bar{y}$	y	$\bar{y}$	x	x	$\bar{x}$	$\bar{x}$	z	$\bar{z}$	$\bar{z}$	z
z	$\bar{z}$	$\bar{z}$	z	y	$\bar{y}$	$\bar{y}$	y	x	$\bar{x}$	x	$\bar{x}$

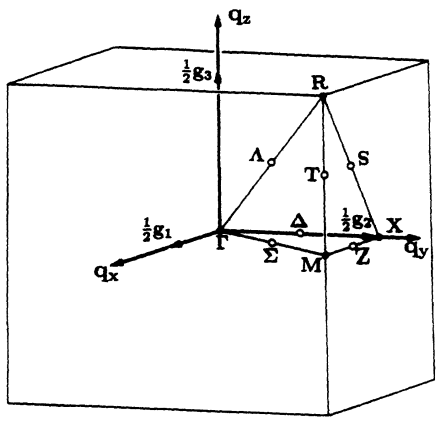

FIG. 3. First Brillouin zone of a simple cubic lattice, showing the points and lines of high symmetry pertinent to the present calculations. $\Gamma = (0,0,0)$, $X = (0,\frac{1}{2},0)$, $M = (\frac{1}{2},\frac{1}{2},0)$, $R = (\frac{1}{2},\frac{1}{2},\frac{1}{2})$ in units of $(\frac{2\pi}{a})$.

according to Koster;[29] the second column gives the corresponding point groups $\mathbf{G(q)}$; the third column gives the dimension of the irreducible representations of group $\mathbf{G(q)}$; the fourth column gives the extradegeneracy due to time-reversal symmetry if any; the fifth column gives the irreducible decomposition of normal modes into different branches. The degeneracy of each branch is indicated in the parentheses. The irreducible representations for $\mathbf{G(q)}$ can be found in Ref. 30.

IV. RESULTS AND DISCUSSION

In this section we discuss our numerical results. In Sec. IV A we give the libron and phonon dispersion relations in the direction of high-symmetry lines in BZ (Fig. 3) and we use these results to calculate the elastic constants. The density of states with and without inclusion of libron–phonon interactions is given in Sec. IV B. Optical and scattering properties are considered in Sec. IV C.

A. Dispersion curves

The dispersion curves for six relevant directions in the Brillouin zone obtained from potential II are shown in Figs. 5(a)–5(e). In order to make a comparison between the two models, we also present the phonon and libron dispersion curves of potential I in Figs. 4(a) and 4(b). These curves are exactly the same as those in Ref. 12.

The representations to which the modes belong at $\mathbf{q} = 0$ (factor group T_h) are indicated in the figures. The translations are odd under inversion and the number of lattice translation is given by

$$\Gamma_T = A_u + E_u + 3T_u. \tag{26}$$

Subtracting acoustic modes $\Gamma_{T_{ac}} = T_u$ (which correspond to the translation of the crystal as a whole), we get

$$\Gamma_T = A_u + E_u + 2T_u. \tag{27}$$

The librations are even and given by

$$\Gamma_R = A_g + E_g + 3T_g. \tag{28}$$

Thus at point Γ, we have pure five translational and five librational modes with one onefold, one twofold, and three threefold degeneracies. From Fig. 4(a) we see that potential I does not give this result. There is a nearly accidental fivefold degeneracy. As shown in Fig. 5(a) there are no accidental degeneracies for potential II. For the phonons at this point both potential models give results as expected from group theory. The main difference is the lowest-energy mode which is A_u for potential I while T_u for potential II. At this point, all libron modes are Raman active, while only T_u modes (except acoustic modes) are IR active. However, due to the high symmetry of C_{60} the observation of libron modes by a Raman experiment may not be practically possible. In Appendix B we present the more detailed study of these modes from purely symmetry arguments, like explicit expressions for eigenvalues, eigenvectors, and the most simplified form of the dynamical matrix.

For the $\Delta(0,\alpha,0)$ direction, the group of the $\mathbf{q}$ vector is isomorphic to $C_{2v}(y)$ and as a result all degeneracy is supposed to be removed. We have four different representations $\Delta_1, \Delta_2, \Delta_3, \Delta_4$. As we see from Figs. 4(a) and 5(a) the libron dispersion curves from both potentials are all nondegenerate as occurred in group theory. For the phonon dispersion curves in this direction, potential I has two twofold nearly accidental degenerate branches; one is the highest-energy optical mode and the

TABLE III. High-symmetry points and lines in the BZ and the elements of T_h that leave the wave vector fixed or changed by a vector of the reciprocal lattice. The symmetry operations R_k are given explicitly in Appendix A.

High symmetry points and lines in BZ		Elements of T_h that leave $\mathbf{q}$ invariant
$\mathbf{\Gamma}$	(0,0,0)	$R_1, ..., R_{24}$
X	(0,1,0)	$R_1, R_7, R_{13}, R_{19}, R_4, R_{10}, R_{16}, R_{23}$
M	(1,1,0)	$R_1, R_7, R_{13}, R_{19}, R_4, R_{10}, R_{16}, R_{23}$
R	(1,1,1)	$R_1, ..., R_{24}$
$\mathbf{\Delta(\Gamma X)}$	$(0,\alpha,0)$	$R_1, R_{13}, R_{10}, R_{22}$
$\mathbf{\Sigma(\Gamma M)}$	$(\alpha,\alpha,0)$	R_1, R_{10}
$\mathbf{\Lambda(\Gamma R)}$	(α,α,α)	R_1, R_2, R_3
S(XR)	$(\alpha,1,\alpha)$	R_1, R_{16}
Z(XM)	$(\alpha,1,0)$	$R_1, R_{19}, R_{16}, R_{20}$
T(MR)	$(1,1,\alpha)$	R_1, R_7, R_{16}, R_{22}

TABLE IV. Group-theoretical analysis of C_{60}, as explained in the text.

Points q		Point symmetry G(q)	Dimension of irr. representation	Time reversal degeneracy	Number of branches and degeneracy
Γ	(0,0,0)	T_h	1	no	2(1)+2(2)+6(3)
X	(0,1,0)	D_{2h}	2	no	12(2)
M	(1,1,0)	D_{2h}	2	yes	6 (4)
R	(1,1,1)	T_h	2	yes	6 (4)
Δ(ΓX)	$(0,\alpha,0)$	$C_{2v}(y)$	1	no	24(1)
Σ(ΓM)	$(\alpha,\alpha,0)$	$C_s(z)$	1	no	24(1)
Λ(ΓR)	(α,α,α)	C_3	1	no	8(1) + 8(2)
S(XR)	$(\alpha,1,\alpha)$	$C_s(y)$	1	yes	12(2)
Z(XM)	$(\alpha,1,0)$	$C_{2v}(x)$	1	yes	12(2)
T(MR)	$(1,1,\alpha)$	$C_{2v}(z)$	2	yes	6 (4)

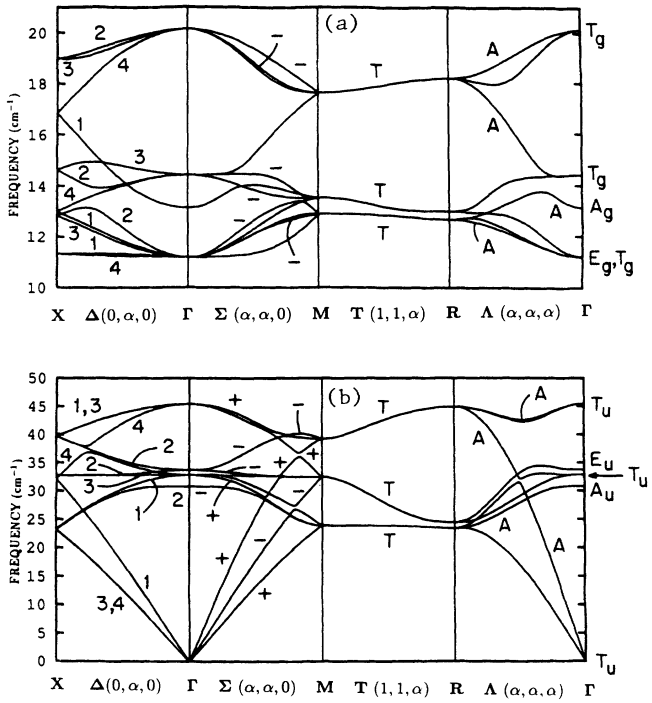

FIG. 4. (a) Top: Harmonic libron dispersion curves obtained from potential I (in the absence of phonon–libron interaction) in the directions $X \rightarrow \Gamma, \Gamma \rightarrow M, M \rightarrow R$, and $R \rightarrow \Gamma$. Curves are labeled by the irreducible representations according to which the wave functions transform. Along $\Delta(0,\alpha,0)$ the labels 1, 2, 3, and 4 denote the representations Δ_1, Δ_2, Δ_3, and Δ_4, respectively. Along $\Sigma(\alpha,\alpha,0)$, the minus sign indicates modes which are odd under the glide-plane operation R_{10} of Appendix A. Modes which are unlabeled in this direction are even under R_{10}. Along $T(1,1,\alpha)$ all modes transform according to the representation T. Along $\Lambda(\alpha,\alpha,\alpha)$ modes are labeled according to how they transform with respect to the threefold axis. Modes labeled A transform according to the identity representation. The unlabeled modes transform according to the two complex conjugate E representations, which are degenerate. The symmetry of the modes at $\Gamma(0,0,0)$ is indicated in the right-hand margin and is discussed in detail in Appendix B. (b) Bottom: Harmonic phonon dispersion curves for potential I, as in (a). Along $\Sigma(\alpha,\alpha,0)$ the modes which are even under R_{10} are explicitly labeled +.

other is the lowest-energy acoustic mode, while potential II has no such accidental degeneracy [Figs. 4(b) and 5(b)]. The other important remark is the small splitting of the branches along this direction, as shown in Fig. 5(b), which are proportional to the order parameter. Consequently, these splittings disappear in the orientationally disordered fcc phase due to the higher symmetry. As shown in Fig. 4(b), these splittings are negligibly small in the case of potential I. In this regard potential I appears to be more symmetric than the crystal structure requires. Also, we note that the effect of the libron–phonon interaction is stronger in this direction than in the other symmetry directions. Thus in Fig. 5(e) we see relatively large splittings in the $\Delta(0,\alpha,0)$ direction at the places where either the longitudinal or transverse phonons cross the librons dispersion curves. At point $X = (0,1,0)$, due to the time-reversal degeneracy each branch is twofold degenerate and this is the case for both models even though the lowest-energy phonon modes of potential I are almost fourfold degenerate.

For the $\Sigma(\alpha,\alpha,0)$ direction, only a glide mirror plane is preserved and the group of the q vector is isomorphic to $C_s(z)$. Now, only two representations Σ_1 and Σ_2 occur and the large number of branches which arise in the absence of degeneracy interact (acoustic modes interact with the optical modes) and give rise to a very complex pattern for both potential models. At point M(1,1,0) we have fourfold degeneracy which is caused by self-stocking of the branches. Along Σ and at the point M translational and librational motions are mixed.

Along the direction $T(1,1,\alpha)$ and at point $R = (1,1,1)$ the fourfold degeneracy is preserved. While translational and librational modes are mixed along T, they are separated into pure translational and pure librational modes at point R (belonging to the R_1 and R_2 irreducible representation, respectively). For the phonon-dispersion curves obtained from potential II there is a eightfold nearly accidental degenerate branch at point R [Fig. 5(b)]. Including next-nearest-neighbor interaction, this degeneracy may be removed.

For the direction $\Lambda(\alpha,\alpha,\alpha)$, only threefold rotation axis is preserved and thus the group of the q vector is isomorphic to C_3 and as a result only two representations occur; one double degenerate (labeled $E = \{\Lambda_2, \Lambda_3\}$) and the other nondegenerate (labeled $A = \Lambda_1$). The

double degenerate is caused by time-reversal symmetry. It is important to note that the acoustic branches have large dispersion and in the absence of libron–phonon interactions the nondegenerate acoustic branch A interacts with the corresponding optic branch arising from T_u and A_u at $\mathbf{q} = \mathbf{0}$ for potentials I and II, respectively. Also, for both potential models, the previously pure librational branches at point R are split up and cover a wider range of frequencies as we go to Γ along Λ. This change is strongly reflected in the density of states shown in Figs. 7 and 8.

Along other directions $Z(1,\alpha,0)$ and $S(\alpha,1,\alpha)$, due to the time-reversal degeneracy all branches are twofold degenerate as obtained from both potentials [Figs. 5(c)–5(d)].

From these dispersion curves shown in Figs. 4(a) and

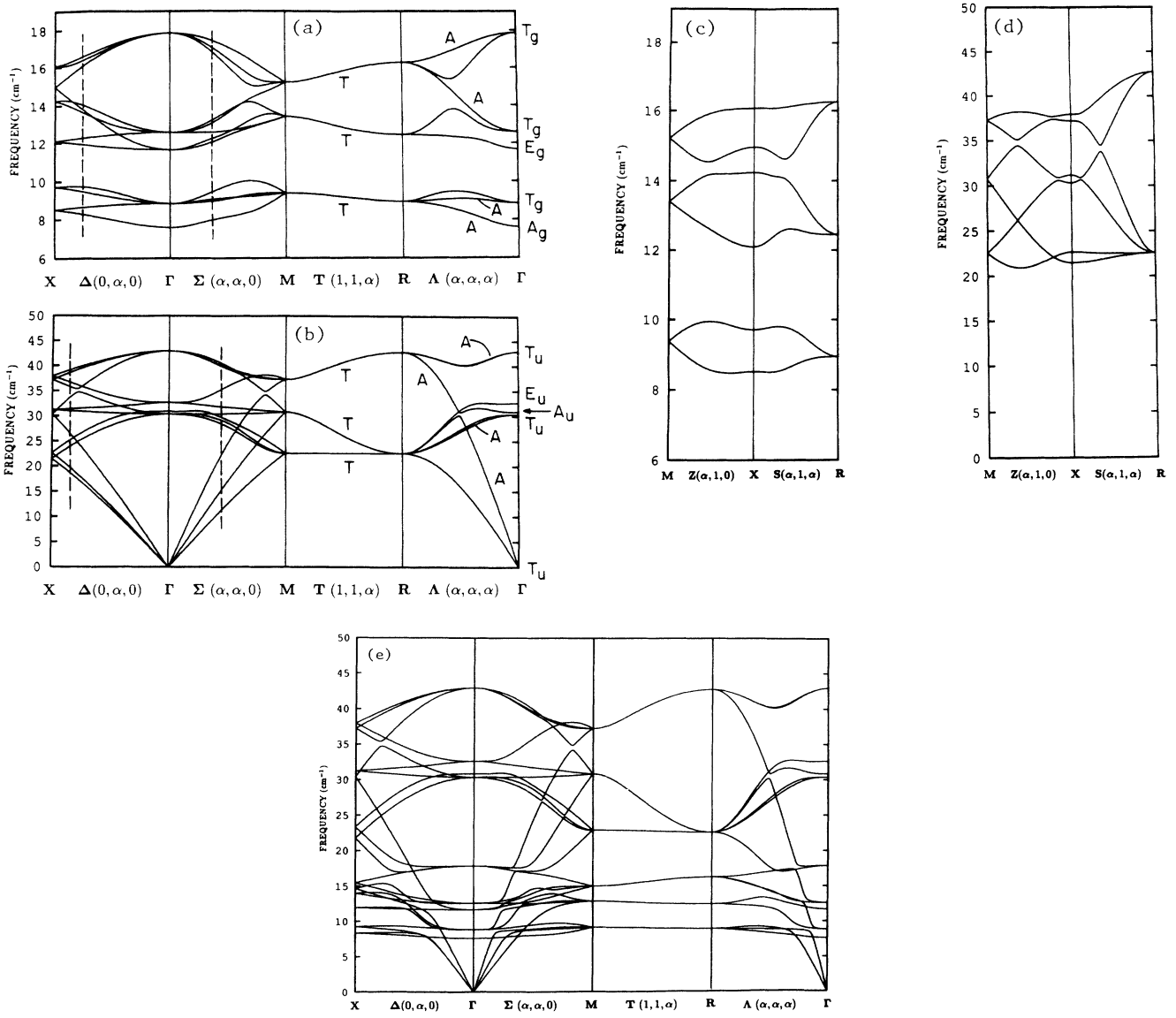

FIG. 5. (a) Harmonic libron dispersion curves obtained from potential II (in the absence of phonon–libron interaction) in the directions $X \to \Gamma, \Gamma \to M, M \to R$, and $R \to \Gamma$. The notation for the symmetry labels is the same as in Fig. 4. Along $\Delta(0,\alpha,0)$ the symmetry labels in increasing order of frequency (along the dashed line) are (1, 4, 3, 2, 1, 4, 2, 1, 3, 4, 3, 2). Along $\Sigma(\alpha,\alpha,0)$ the symmetry labels in increasing order of frequency (along the dashed line) are $(+,+,-,-,+,+,-,+,-,-,+,-)$. (b) Harmonic phonon dispersion curves for potential II, as in (a). Along $\Delta(0,\alpha,0)$ the symmetry labels in increasing order of frequency (along the dashed line) are (4, 3, 1, 2, 1, 3, 2, 4, 4, 2, 1, 3). Along $\Sigma(\alpha,\alpha,0)$ the symmetry labels in increasing order of frequency (along the dashed line) are $(+,-,+,+,-,-,+,-,-,+,-,+)$. (c) Harmonic libron dispersion curves obtained from potential II (in the absence of phonon–libron interaction) in the directions $M \to X$ and $X \to R$. (d) Harmonic phonon dispersion curves obtained from potential II as in (c). (e) Harmonic libron and phonon dispersion curves obtained from potential II (in the presence of phonon-libron interaction) in the directions $X \to \Gamma, \Gamma \to M, M \to R$, and $R \to \Gamma$.

TABLE V. Sound velocities along various high-symmetry directions and elastic constants obtained from both potential models.

Propagation directions	Sound velocities (km/s)							Elastic constants (Mbar)		
	[100][a]		[110]			[111]				
	c_t	c_l	c_{t_1}[b]	c_{t_2}[c]	c_l	c_t	c_l	c_{11}	c_{12}	c_{44}
Potential I	2.17	2.93	1.54	2.17	3.31	1.77	3.43	0.149	0.069	0.081
Potential II	2.10	2.84	1.52	2.10	3.19	1.74	3.30	0.141	0.060	0.077

[a]Along this direction we have two nondegenerate transverse acoustic branches. However, as discussed in the text, the two transverse mode energies have the same slope in the long-wavelength limit, so that number of elastic constants is still 3, as expected for cubic symmetry.

[b]This is the transverse mode having displacements in the xy plane.

[c]This is the transverse mode whose displacements are perpendicular to the xy plane.

4(b) and Figs. 5(a)–5(e) the main conclusion made is that potential model I is more symmetric than model II in the sense that model I gives rise to nearly accidental degeneracy at many points and lines.

The other interesting remark concerns potential II. Note that the upper two libron bands in Fig. 5(a) are surprisingly similar to the entire libron spectrum of solid H_2,[19] shown in Fig. 6. The lowest band of four libron branches in Fig. 5(a) corresponds predominantly to spinning libration of molecules about their local threefold axis. For diatomic molecules there is no such orientational motion. Thus we cannot expect to see (in Fig. 6) any analog of the lowest band of librons in Fig. 5(a).

Potential II not only gives similar results to that of H_2 for libron dispersion curves but also for phonon-dispersion curves as well as density of states.[20,21] If potential II is the correct model for C_{60} we can expect many similarities in the dynamical properties of C_{60} and H_2. However, we have to take into account the fact that C_{60} is a three-dimensional molecule with much bigger mass and more symmetric structure than that of solid H_2. For instance, for H_2 anharmonic librons play a crucial role in the lattice dynamics while this is not the case for C_{60} due to its big mass.

From the slopes of acoustic phonon modes, one can get the sound velocities from which elastic constants of C_{60} at low temperature are obtained. (This procedure is simpler than an analytic treatment of the acoustic mode energies in the long-wavelength limit.) These results are summarized in Table V. One sees that both potential models give almost the same results. The values of the elastic constants we find are half as large as those given in Ref. 12, possibly indicating that their result is subject to some confusion in the scale of wave vectors.

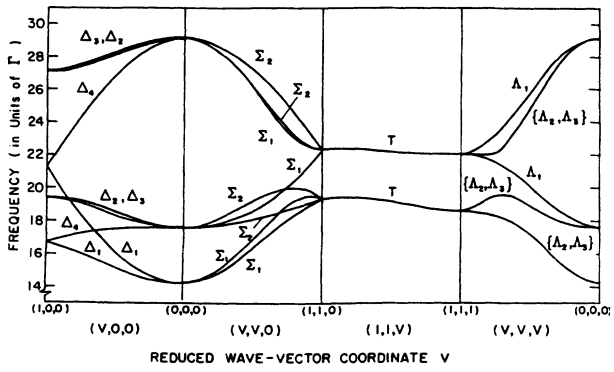

FIG. 6. Harmonic libron dispersion curves along four symmetry directions for solid H_2 taken from Ref. 19.

The above determination of the elastic constants involves the sound velocities in the asymptotic long-wavelength limit. In this limit the sound velocities of the two transverse modes along $\Delta(0,q,0)$ are required to be identical for a cubic crystal. However, this degeneracy of the frequencies of the two transverse modes need not persist to higher than first order in the wave vector q. In particular, for the $Pa3$ space group, these two transverse modes are *not* degenerate, as can be seen in Fig. 5(b) for potential II. [For potential I the removal of degeneracy is too small to be seen in Fig. 4(b).] If the molecular orientations were disordered, we would have an fcc Bravais lattice, for which the transverse modes *are* required to be degenerate for wave vectors along $\Delta(0,q,0)$. Thus the removal of degeneracy is due to sublattice formation caused by orientational ordering and the difference in energy between these two modes must be proportional to the orientational order parameter. In view of the degeneracy in the asymptotic sound velocities, this energy difference must occur at higher than first order in q, i.e., probably at order q^3.

Not all of the results discussed in this section are likely to have an experimental confirmation, at least not until there is an increase in the resolution for neutron-diffraction experiments, since 24 branches in the lattice region lie too close together. Also, a large single crystal of C_{60} will be needed. However, assuming the existence of such a crystal, along the $T(M \rightarrow R)$ lines and at points M and R the fourfold degeneracy makes such an experimental attempt much more reasonable, since not only the separation between branches is fairly large, but the degeneracy should enhance considerably the diffracted intensity. More generally, the symmetry properties we indicate could be helpful in identifying the type of modes.

B. Density of states

Figures 7 and 8 show the density of states of phonon, libron, and phonon–libron (including interaction) obtained

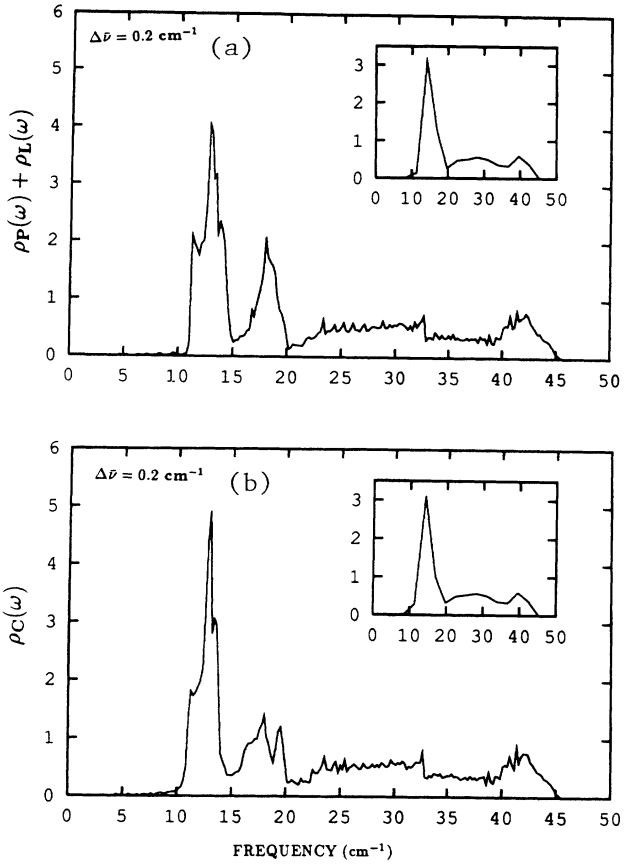

FIG. 7. (a) Top: For potential I, the spectrum $\rho_L(\omega) + \rho_P(\omega)$ in the absence of libron–phonon coupling. The histogram results from sampling 32 768 points in the Brillouin zone. The width of the channels $\Delta\bar{\nu}$ in which the contributions to the density of states is stored is indicated. The vertical axis is defined as $1/N$ times the number of states per unit of frequency where N is the number of unit cells. In inset we present the same spectrum by using wider channels of width 4 $\text{cm}^{-1} \sim 0.5$ meV which is about same order as the experimental resolution normally obtained at present. (b) Bottom: As in (a), for potential I, the spectrum of the combined phonon–libron density of states, $\rho_C(\omega)$, when libron–phonon coupling is included.

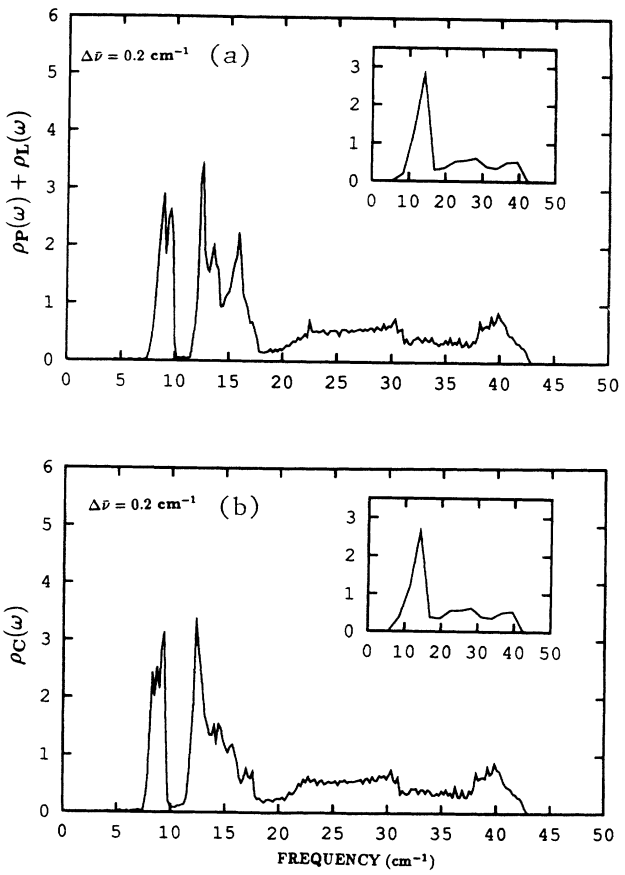

FIG. 8. Same as Fig. 7 but here for potential II.

from both potential models. These curves were obtained by dividing the irreducible part of the BZ into $16\times16\times16$ parallelograms of the same shape as the BZ and then diagonalizing the 24×24 matrix at the wave vector $\mathbf{q}$ in the center of each parallelogram. The width of the channels in which the contributions to the density of states is stored are indicated in Figs. 7 and 8.

For potential model I, Fig. 7(a) shows that the density of states in the absence of interactions is highly double peaked between 11 and 20 cm^{-1}. With the inclusion of interactions [Fig. 7(b)] the second peak gets broader and weaker and also splits up into two small peaks, while the first peak gets narrower and sharper. Its amplitude changes from about 4 to 5. At higher frequencies (higher than 20 cm^{-1}) the interactions have almost no effect, as expected. In the inset of the same figure we present the same density of states with channels of 4 $\text{cm}^{-1} \sim 0.5$ meV width, which is about the same order as experimental resolution. Librons give rise to one strong peak centered around 15 cm^{-1} with width 4 cm^{-1}.

The curves for density of states obtained from potential II are different from the one discussed above. The most important remark about density of states of librons as shown in Figs. 8(a) and 8(b) is that there are almost no states in the region between 10.2 and 11.6 cm^{-1}. This result agrees very well with one given in Ref. 11 in which densities of librons are obtained for 32 molecules via molecular-dynamic simulations. From these figures we see that when there is no interaction, three peaks [corresponding three bands in Fig. 5(a)] can be identified between the ranges 7–10 cm^{-1}, 12–14 cm^{-1}, and 14–18 cm^{-1}. The effect of phonon-libron interactions on these peaks is strong and shown in Fig. 8(b). The peak between 14 and 18 cm^{-1} disappears. In the insets to Figs. 8(a) and 8(b), the same spectrum is shown with a scale of experimental resolution. We have one peak between energies 10 and 18 cm^{-1}.

Recently, well-defined librational excitations have been observed at about 2.5 meV (20 cm^{-1}) (Ref. 31) in the low-temperature ordered phase of solid C_{60}. The sharpness of the peaks indicates that the intermolecular potential does not depend strongly on the axis of the angular displacement. However, from the insets to Figs. 7 and 8

we see that both potential models give a librational band centered at ~ 15 cm^{-1} (1.86 meV) and the width of the band is ~ 4 cm^{-1} (0.5 meV) for potential I and 5 cm^{-1} (0.6 meV) for potential II implying that the orientational potential models are not as symmetric as the results in Ref. 31 indicate.

C. Optical and scattering properties

Here we discuss the observation of the normal modes whose dispersion curves we have given in Figs. 4 and 5 and whose density of states is shown in Figs. 7 and 8. We start by discussing the optical observation of the normal modes. As is well known, infrared absorption may be observed for optical modes at zero wave vector with T_u symmetry. Of course, in the disordered phase, when the system is described by an fcc Bravais lattice, there are no optical modes. Accordingly, in the orientationally disordered phase, we expect no infrared absorption due to processes involving a single intermolecular phonon. (The present discussion is not concerned with intramolecular phonons.) In the ordered phase, we do have optical modes with T_u symmetry. These modes, shown in Figs. 4(b) and 5(b), have energies of order 30–45 cm^{-1}. Furthermore, since the intensities of these absorptions vanish in the disordered phase, we intuit that they are proportional to the square of the order parameter. In the case of orientationally ordered solid N_2, Schnepp[32] showed that the infrared absorption cross section at zero temperature was proportional to the square of the quadrupole moment. More general arguments[33] indicate that the absorption cross section at nonzero temperature is proportional to the square of the (quadrupolar) orientational order parameter. We expect the same type of result to hold here, except that here the order parameter is defined (see Ref. 5) in terms of averages of sums over atoms of sixth-order spherical harmonics. Therefore the measurement of the temperature dependence of the oscillator strength of the optical phonon provides an alternative experimental way to access the temperature dependence of the order parameter.

With regard to Raman scattering, symmetry indicates that the libron modes are in principle observable. In the case of solid N_2 or solid H_2 the mechanism for Raman scattering involves an interaction with the radiation field proportional to αE^2, where α is the polarizability. It is important that the molecular polarizability is anisotropic, and thus depends on the orientation of the diatomic molecules. Expanding this orientational dependence in terms of libron amplitudes shows that in Raman scattering one can observe creation of single libron modes at zero wave vector. (Anharmonic libron–libron interactions permit creation of two librons during Raman scattering.[34]) But here, the molecular polarizability, being a second-rank tensor, is isotropic, at least if distortions of the molecule away from icosahedral symmetry are neglected. Thus, in the independent molecule approximation, the polarizability is independent of libron amplitudes, and hence gives rise to no Raman scattering due to librons. However, in principle there will be a small anisotropy in the polarizability due to the multipole field of one molecule acting on its neighbors. When the multipoles are dipoles, this effect is called the dipole–induced-dipole mechanism.[35] Such a mechanism might give rise to a Raman cross section from simultaneous creation of one or possibly several librons. We are presently pursuing such calculations.

Recently, van Loosdrecht, van Bentum, and Meijer[36] have performed Raman experiments on single-crystal C_{60} samples. Several of their results are quite provocative. For instance, they see reasonably well-defined features at energies of 56, 80, and 109 cm.$^{-1}$. Since the energy separation between these features is of order 25 cm^{-1}, one is tempted to identify them as arising from multiple libron processes. In such an interpretation these features would represent simultaneous creation of three, four, and five librons, respectively. In this scenario, the two-libron feature might be obscured by the very intense unshifted Lorentzian central peak in their Fig. 5. In view of the libron energies observed by Neumann *et al.*[31] it is less attractive to attribute the three features to two-, three-, and four-phonon processes. Before any definitive interpretation of these results is given, it is clearly important that these results should be confirmed as being intrinsic to bulk solid C_{60}.

With regard to inelastic scattering of neutrons the meaning of our results is rather clear. We would emphasize that by comparing results for different scattering vectors, all of which are equal modulo a vector of the reciprocal lattice could prove interesting. Suppose, for instance, one performs such an experiment for two scattering vectors $\mathbf{K}_1$ and $\mathbf{K}_2$ which are equivalent, i.e., which differ by a vector of the reciprocal lattice. Within a harmonic version of lattice dynamics, the phonon frequencies for these two scattering vectors will be identical. However, their intensities will be proportional to the square of the magnitude of the Fourier transform of the phonon polarization vector within the unit cell. Thus by comparing intensities at several such equivalent scattering vectors it should be possible to recover information on the phonon polarization vector of each modes. This type of analysis could be done both at zero wave vector (for optical modes) and at nonzero wave vector.

V. ROOT-MEAN-SQUARE DISPLACEMENTS

In this section we shall discuss the validity of our small-amplitude expansion. For this we first derive a formula for the root mean square of the amplitude of rotational and translational oscillations. After expanding the potential energy of the molecular crystal in terms of $\mathbf{u}^t(\mathbf{a},\mu)$ and $\mathbf{u}^r(\mathbf{a},\mu)$ in the harmonic approximation and then defining the crystal normal coordinates through the linear transformation

$$Q^i_\tau(\mathbf{q}) = \frac{1}{\sqrt{N}} \sum_{a\mu} \sum_{\alpha} E^\tau_{\mu\alpha}(\mathbf{q}) e^{-i\mathbf{q}\cdot\mathbf{X}(\mathbf{a})} u^i_\alpha(a,\mu),$$

$$\alpha = x,y,z, \quad \mu = 1\text{–}4, \quad (29)$$

where $i = t, r$ for translational and librational motions, respectively, the Hamiltonian becomes

$$H = \frac{1}{2} \sum_{i=t,r} \sum_{\mathbf{q}} \sum_{\tau=1}^{12} \{\dot{Q}_\tau^i(\mathbf{q})\dot{Q}_\tau^i(-\mathbf{q}) + \omega_\tau^2(\mathbf{q}) Q_\tau^i(\mathbf{q}) Q_\tau^i(\mathbf{q})\}. \tag{30}$$

Now we are ready to calculate the average root mean square of displacement and libration amplitudes $< t_\alpha(a,\mu)^2 >$, $< \theta_\alpha(a,\mu)^2 >$. Due to the translational symmetry these quantities do not depend on the unit cell indices a. Furthermore, since four sublattices are symmetry related, the averages do not depend on the sublattice indices μ either. Finally, due to the site symmetry $S_6(\bar{3})$, $< t_\alpha(a,\mu)^2 >$ and $< \theta_\alpha(a,\mu)^2 >$ do not depend on the Cartesian components $\alpha = x, y, z$. Thus we shall calculate the following quantities:

$$< \boldsymbol{\theta}^2 > = < \theta_x^2 + \theta_y^2 + \theta_z^2 > = \frac{1}{4}\frac{1}{N} \sum_a \sum_\mu \sum_\alpha < \theta_\alpha(a,\mu)^2 >, \tag{31}$$

$$< \mathbf{t}^2 > = < t_x^2 + t_y^2 + t_z^2 > = \frac{1}{4}\frac{1}{N} \sum_a \sum_\mu \sum_\alpha < t_\alpha^2(a,\mu) > . \tag{32}$$

Using the notation $< \mathbf{U}^{i2} >$, $i = t, r$ for $< \mathbf{t}^2 >$ and $< \boldsymbol{\theta}^2 >$, respectively, and Eqs. (2) and (3), we get

$$< \mathbf{U}^{i2} > = \frac{1}{4}\frac{1}{N} \sum_a \sum_\mu \sum_\alpha \frac{1}{m^i} < u_\alpha^i(a,\mu)^2 >, \tag{33}$$

where $m^i = M, I$ for $i = t, r$.

From inverse transformation of Eq.(29) and using orthogonality of the eigenvectors $E_{\mu\alpha}^\tau(\mathbf{q})$ we get

$$< \mathbf{U}^{i2} > = \frac{1}{4}\frac{1}{N} \sum_{\mathbf{q}} \sum_\tau \frac{1}{m^i} < Q_\tau^i(\mathbf{q}) Q_\tau^i(-\mathbf{q}) > . \tag{34}$$

From this equation it is possible to estimate the averages as a function of temperature. For this from the Hamiltonian in Eq. (30) we equate the mean potential energy of each normal mode to one-half the mean total energy of a quantum oscillator of the same frequency,

$$\frac{1}{2}\omega_\tau^2(\mathbf{q}) < Q_\tau^i(\mathbf{q}) Q_\tau^i(-\mathbf{q}) > = \frac{1}{2}\hbar\omega_\tau(\mathbf{q}) \left[n + \frac{1}{2} \right], \tag{35}$$

where $n = (e^{\hbar\omega_\tau/kT} - 1)^{-1}$. Thus by substituting this in Eq. (34) we get

$$< \mathbf{U}^{i2} > = \frac{1}{8}\frac{1}{N} \sum_{\mathbf{q}} \sum_\tau \frac{\hbar}{m^i \omega_\tau(\mathbf{q})} \coth\left(\frac{\hbar\omega_\tau}{2kT} \right), \tag{36}$$

which, for potential model II, at zero temperature gives the following results:

$$< \boldsymbol{\theta}^2 > = \frac{1}{8} \left(\frac{h}{4\pi^2 I} \right) \frac{1}{N} \sum_{\mathbf{q}} \sum_\tau \frac{1}{\nu_\tau(\mathbf{q})} = (1.50°)^2 \tag{37}$$

and

$$< \mathbf{t}^2 > / R^2 = \frac{1}{8} \left(\frac{h}{4\pi^2 M} \right) \frac{1}{N} \sum_q \sum_\tau \frac{1}{\nu_\tau(\mathbf{q})} = (0.0049)^2, \tag{38}$$

where $R = a/\sqrt{2}$ is the distance between nearest-neighbor molecules in the crystal. Due to the big mass of C_{60} these values are very small indicating that harmonic approximation is a very good approximation for solid C_{60}. For other temperatures the values of $\sqrt{< \mathbf{t}^2 >}$ and $\sqrt{< \boldsymbol{\theta}^2 >}$ are given in Table VI for both potential

TABLE VI. Estimates of $\sqrt{< \mathbf{t}^2 >}/R$ (where $R = a/\sqrt{2}$ is the nearest-neighbor distance) and $\sqrt{< \theta^2 >}$ as a function of temperature for potentials I and II. The values of the lattice constants, a, at different temperatures are taken from Ref. 8.

Temperature	Lattice constant	Potential I		Potential II	
(K)	(Å)	$\sqrt{< \mathbf{t}^2 >}/R$	$\sqrt{< \theta^2 >}$	$\sqrt{< \mathbf{t}^2 >}/R$	$\sqrt{< \theta^2 >}$
0	14.041	0.0048	1.39°	0.0050	1.45°
20	14.043	0.0054	2.03°	0.0057	2.36°
50	14.048	0.0075	3.10°	0.0079	3.64°
115	14.060	0.0115	4.77°	0.0122	5.67°
T_c[a]	14.101	0.0185	7.50°	0.0195	9.15°
300[b]	14.160	0.0219		0.0232	
1000[b,c]	14.335	0.0548		0.0578	
1500[b,c]	14.460	0.0866		0.0910	
1650[b,c]	14.498	0.0988		0.1043	
1800[b,c]	14.535	0.1130		0.1193	
2000[b,c]	14.585	0.1363		0.1439	

[a]These data are meant to be associated with the orientationally ordered phase just at the orientational ordering transition. We used the value $T_c = 260$ K according to Ref. 8.

[b]For $T > T_c$ there is no long-range orientational order and thus $(< \theta^2 >)^{1/2}$ is meaningless.

[c]The lattice constant at this temperature is estimated by linear extrapolation of the data in Ref. 8 between temperatures $T = 300$ K and $T = 2000$ K.

models. At T= 115 K, for potential II $\sqrt{<\theta^2>}$ is 5.67°, which agrees very well with the experimental value 5.7.[31] As shown in Table VI, the mean-square values obtained from potential II are slightly larger than those of potential I, which is consistent with the values of transition temperature obtained from both potential models. For instance, T_c is 215 K for potential II (Ref. 11) and 270 K for potential I,[10] while the experimental values 250 K (Ref. 1) and 260 K (Ref. 8) are somewhat between these two values. At temperatures $T > T_c$ we do not have orientational order and thus one should use the isotropic part of the potential models to estimate the mean-square values of the translational displacements. However, as we have seen in the preceding section the orientational dependence of the potential only causes a small splitting of the branches [Fig. 5(b)] and thus it is still a good approximation to use it in calculation of $\sqrt{<\mathbf{t}^2>}$. Within this approximation, at temperature 1650 K $\sqrt{<\mathbf{t}^2>}/R$ is ~0.1, and thus according to the Lindemann criterion, the melting point of solid C_{60} is around 1700 K. Even though the validity of Lindemann criterion is not well defined for such large molecules where the size of molecule is almost 1/3 of the distance between the center of two molecules, this value is of the correct order of magnitude.[37]

VI. CONCLUSION

In this paper we have studied the lattice dynamics of solid C_{60} within the harmonic approximation and reached the following conclusions.

(1) Both of the recently proposed potential models give almost the same result for phonon modes while potential II gives a slightly lower libron frequencies. Nevertheless, according to the experimental data in Ref. 31 both potentials need to be somewhat modified in their orientational dependence.

(2) We showed that the quasiharmonic approximation (based on harmonic phonons in a crystal with a temperature-dependent lattice constant) is valid up to about 1000 K for phonon modes. (The criterion we used for the validity of the harmonic approximation was that the root-mean-square displacement was 5% of the separation between centers of nearest-neighboring molecules.) Thus the temperature dependence of many quantities, such as the elastic constants, energy spectrum, etc. can be calculated by simply assuming the only effect of temperature is to change the lattice constant.

(3) In Table V we give values for the elastic constants from the calculated sound velocities. These values represent corrections from the results of Ref. 12.

(4) We give the symmetry labels of the libron and phonon modes for the wave vector along high-symmetry directions. This information is useful in considering optical properties of zero-wave-number modes and might even aid in the identification of modes obtained by inelastic neutron scattering.

(5) From purely symmetry arguments we showed that the dynamical matrix depends on only eight independent parameters to describe the orientational dependence and five independent parameters to describe the center-of-mass dependence of the elastic potential energy.

(6) At $\mathbf{q} = \mathbf{0}$ the dynamical matrix reduces to block diagonal form in which A and E symmetry blocks are one dimensional and T symmetry blocks are three dimensional. We also gave the 24 symmetry-adapted vectors and expressions for the energies of libron and phonon modes as a function of any given potential model at this point. Such information is most valuable not only for the quick test of new potential models but also for the analysis of the infrared, Raman, and neutron scattering of the crystal.

(7) Using the Lindemann criterion, we estimate the melting temperature of solid C_{60} from these potentials to be about 1700 K.

(8) Observation of single-libron excitations via Raman scattering is problematic in view of the nearly spherical symmetry of the molecules. However, it is possible that one might observe multiple libron processes involving higher multipole generalizations of the dipole–induced-dipole[35] mechanism. Such a mechanism might explain the features observed by van Loosdrecht, van Bentum, and Meijer[36] in their single-crystal Raman experiments near 100 cm^{-1}. However, before accepting such an explanation, it is important that these Raman features be confirmed as being intrinsic to bulk C_{60}. If so, they may arise from processes involving simultaneous creation of three, four, and five librons.

ACKNOWLEDGMENTS

We acknowledge helpful conversations with P. A. Heiney and E. J. Mele. This work was supported in part by the National Science Foundation under Grant No. NSF-88-15469. We also acknowledge partial support from the National Science Foundation under the Materials Research Laboratory program, Grant No. DMR88-19885. Some of the computations were supported by a grant from the Research Foundation of the University of Pennsylvania.

APPENDIX A: MATRIX REPRESENTATION OF GROUP ELEMENTS

In this appendix we give the matrix form of 24 elements of the group T_h together with the corresponding fractional translation. Note that trace of the matrices $E, C_{3\mu}^{\pm}, S_{6\mu}^{\pm}$ that leave one of the sublattices unchanged (see Table II) are all zero except $R_1 = E$. Thus from Eq. (25) we get $\chi(\mathbf{q}; R_1) = 24$ and $\chi(\mathbf{q}; R_i) = 0$ for R_i =*other elements of* $\mathbf{G}(\mathbf{q})$. Now from Eq. (23) decomposition of the reducible representation of the $\mathbf{G}(\mathbf{q})$ can be easily obtained as shown in Table IV.

(a) $\mathbf{V}(\mathbf{R}) = (0,0,0)$:

$$R_1 = \mathbf{E} = \begin{bmatrix} 1&0&0 \\ 0&1&0 \\ 0&0&1 \end{bmatrix}, \quad R_2 = \mathbf{C}_{31}^{+} = \begin{bmatrix} 0&0&1 \\ 1&0&0 \\ 0&1&0 \end{bmatrix}, \quad R_3 = \mathbf{C}_{31}^{-} = \begin{bmatrix} 0&1&0 \\ 0&0&1 \\ 1&0&0 \end{bmatrix}, \tag{A1}$$

$$R_4 = \mathbf{I} = \begin{bmatrix} \bar{1}00 \\ 0\bar{1}0 \\ 00\bar{1} \end{bmatrix}, \quad R_5 = \mathbf{S}_{61}^{-} = \begin{bmatrix} 00\bar{1} \\ \bar{1}00 \\ 0\bar{1}0 \end{bmatrix}, \quad R_6 = \mathbf{S}_{61}^{+} = \begin{bmatrix} 0\bar{1}0 \\ 00\bar{1} \\ \bar{1}00 \end{bmatrix}. \tag{A2}$$

(b) $\mathbf{V}(\mathbf{R}) = \mathrm{a}\,(\frac{1}{2}, 0, \frac{1}{2})$:

$$R_7 = \mathbf{C}_{2z} = \begin{bmatrix} \bar{1}00 \\ 0\bar{1}0 \\ 001 \end{bmatrix}, \quad R_8 = \mathbf{C}_{34}^{+} = \begin{bmatrix} 00\bar{1} \\ \bar{1}00 \\ 010 \end{bmatrix}, \quad R_9 = \mathbf{C}_{33}^{-} = \begin{bmatrix} 0\bar{1}0 \\ 00\bar{1} \\ 100 \end{bmatrix}, \tag{A3}$$

$$R_{10} = \sigma_z = \begin{bmatrix} 100 \\ 010 \\ 00\bar{1} \end{bmatrix}, \quad R_{11} = \mathbf{S}_{64}^{-} = \begin{bmatrix} 001 \\ 100 \\ 0\bar{1}0 \end{bmatrix}, \quad R_{12} = \mathbf{S}_{63}^{+} = \begin{bmatrix} 010 \\ 001 \\ \bar{1}00 \end{bmatrix}. \tag{A4}$$

(c) $\mathbf{V}(\mathbf{R}) = \mathrm{a}\,(0, \frac{1}{2}, \frac{1}{2})$:

$$R_{13} = \mathbf{C}_{2y} = \begin{bmatrix} \bar{1}00 \\ 010 \\ 00\bar{1} \end{bmatrix}, \quad R_{14} = \mathbf{C}_{32}^{+} = \begin{bmatrix} 00\bar{1} \\ 100 \\ 0\bar{1}0 \end{bmatrix}, \quad R_{15} = \mathbf{C}_{34}^{-} = \begin{bmatrix} 0\bar{1}0 \\ 001 \\ \bar{1}00 \end{bmatrix}, \tag{A5}$$

$$R_{16} = \sigma_y = \begin{bmatrix} 100 \\ 0\bar{1}0 \\ 001 \end{bmatrix}, \quad R_{17} = \mathbf{S}_{62}^{-} = \begin{bmatrix} 001 \\ \bar{1}00 \\ 010 \end{bmatrix}, \quad R_{18} = \mathbf{S}_{64}^{+} = \begin{bmatrix} 010 \\ 00\bar{1} \\ 100 \end{bmatrix}. \tag{A6}$$

(d) $\mathbf{V}(\mathbf{R}) = \mathrm{a}\,(\frac{1}{2}, \frac{1}{2}, 0)$:

$$R_{19} = \mathbf{C}_{2x} = \begin{bmatrix} 100 \\ 0\bar{1}0 \\ 00\bar{1} \end{bmatrix}, \quad R_{20} = \mathbf{C}_{33}^{+} = \begin{bmatrix} 001 \\ \bar{1}00 \\ 0\bar{1}0 \end{bmatrix}, \quad R_{21} = \mathbf{C}_{32}^{-} = \begin{bmatrix} 010 \\ 00\bar{1} \\ \bar{1}00 \end{bmatrix}, \tag{A7}$$

$$R_{22} = \sigma_x = \begin{bmatrix} \bar{1}00 \\ 010 \\ 001 \end{bmatrix}, \quad R_{23} = \mathbf{S}_{63}^{-} = \begin{bmatrix} 00\bar{1} \\ 100 \\ 010 \end{bmatrix}, \quad R_{24} = \mathbf{S}_{62}^{+} = \begin{bmatrix} 0\bar{1}0 \\ 001 \\ 100 \end{bmatrix}. \tag{A8}$$

APPENDIX B: GROUP THEORY OF C_{60} AT $\Gamma(\mathbf{q} = \mathbf{0})$

In the text we have seen that the calculations of external modes of C_{60} in $Pa3$ structure requires the diagonalization of the 24×24 matrix. Considerable help in accomplishing this can be had, however, using group theory. Besides simplifying the diagonalization of the dynamical matrix $\mathbf{D}(\mathbf{q})$, group theory is also of value in classifying and labeling the various modes. The present section is devoted to a discussion of these topics at the point $\Gamma(\mathbf{q} = \mathbf{0})$.

Since C_{60} is a spherical top, for convenience we shall choose the principal axes to be parallel to the crystal-fixed Cartesian axes illustrated in Fig. 3. Furthermore, we shall use the fact that there is no coupling between phonons and librons at Γ and write the 24×24 dynamical matrix as

$$D(\Gamma) = \begin{bmatrix} D^{tt}(\Gamma) & 0 \\ 0 & D^{rr}(\Gamma) \end{bmatrix}, \tag{B1}$$

where

$$D^{ii}(\Gamma) = \begin{bmatrix} D^{ii}(\Gamma, 11) & \cdots & D^{ii}(\Gamma, 14) \\ \vdots & & \vdots \\ D^{ii}(\Gamma, 41) & \cdots & D^{ii}(\Gamma, 44) \end{bmatrix}, \quad i = t, r, \tag{B2}$$

with the 3×3 matrices $D^{ii}(\Gamma, \mu\nu)$,

$$D^{ii}_{\alpha,\beta}(\Gamma, \mu\nu) = \sum_{b\lambda} \Phi^{ii}_{\alpha\beta}(o\mu; b\lambda),$$
$$\Phi^{ii}_{\alpha\beta}(o\mu; b\lambda) = \frac{1}{m^i} \left(\frac{\partial^2 \Phi(o\mu, b\lambda)}{\partial u^i_\alpha(o, \mu) \partial u^i_\beta(b, \nu)} \right)_o . \tag{B3}$$

Consider now the classification of the modes at Γ. This requires first the construction of the set of 12×12 matrices

$$T(\Gamma; R) = \begin{bmatrix} \Lambda(11)R & \cdots & \Lambda(14)R \\ \vdots & & \vdots \\ \Lambda(41)R & \cdots & \Lambda(44)R \end{bmatrix}, \tag{B4}$$

where $\Lambda(\mu\nu) = \delta(\mu, F(\nu, R))$ is given in Eq. (22) and R is an element of T_h and given in Appendix A.

As an illustration, we construct the matrix $T(\Gamma; R)$ for $R = R_2 = C_{31}^{+}$. From Table II we see that under the symmetry operation R_2 the sublattices $\mu = 1, 2, 3$, and 4 goes to $\nu = 1, 4, 2$, and 3, respectively. Thus using Eqs. (B4) and (22), one can easily get

$$T(\Gamma; R_2) = \begin{bmatrix} R_2 & 0 & 0 & 0 \\ 0 & 0 & R_2 & 0 \\ 0 & 0 & 0 & R_2 \\ 0 & R_2 & 0 & 0 \end{bmatrix}, \tag{B5}$$

where R_2 is the 3×3 matrix given in Appendix A. Similarly, other matrices can be constructed. After having done this, the trace of these matrices are easily determined to be

$$\chi(\Gamma; R_1) = 12, \quad \chi(\Gamma; R_i) = 0, \quad i = 2, \ldots, 24. \tag{B6}$$

The decompositions of $S(\Gamma) = \{S(\Gamma; R) \mid R \in T_h\}$ are now immediately obtained using the reduction formula Eq. (23),

$$c_{A_g} = 1, \quad c_{E_g} = 1, \quad c_{T_g} = 3, \tag{B7}$$

$$c_{A_u} = 1, \quad c_{E_u} = 1, \quad c_{T_u} = 3, \tag{B8}$$

and thus 24 modes are divided into pure translational and pure librational modes,

$$\Gamma_{\text{lib}} = A_g + E_g + 3T_g, \tag{B9}$$

$$\Gamma_{\text{trans}} = A_u + E_u + 3T_u. \tag{B10}$$

Above, one of the T_u modes corresponds to the acoustic modes in which the whole lattice translates together and thus may be ignored. The other two T_u modes are IR active while all librational modes are in principle Raman active. However, due to the high symmetry of the molecules, it may not be possible to observe these modes in practice. Since in the decompositions given above, A_g and E_g modes occur once and T_g three times, the librational part of the dynamical matrix (same for phonon part too) can be put into block diagonal form with three 1×1 and three 3×3 matrices. We shall therefore be able to get explicit expressions for the energies of the A_g and E_g modes. For the energies of T_g modes we have to diagonalize 3×3 matrix which is much simpler than diagonalizing 12×12 matrix.

In order to get the information mentioned above we now take up the construction of the symmetry vectors. This is done through the use of the projection operator technique. First we shall consider the projection operator for the A_g mode

$$P(A_g) = \sum_{R \epsilon G_o(\Gamma)} \chi^*(A_g; R) T(\Gamma; R). \tag{B11}$$

The quantity $\chi(A_g; R)$ is the character corresponding to element R in the irreducible representation A_g and is equal to 1. Thus using the matrices $T(\Gamma; R)$ defined in Eq. (B4) it is easily seen that

$$P(A_g) = \begin{bmatrix} (R_1 + R_2 + R_3) & (R_7 + R_{15} + R_{20}) & (R_8 + R_{13} + R_{21}) & (R_9 + R_{14} + R_{19}) \\ (R_7 + R_8 + R_9) & (R_1 + R_{14} + R_{21}) & (R_2 + R_{15} + R_{19}) & (R_3 + R_{13} + R_{20}) \\ (R_{13} + R_{14} + R_{15}) & (R_3 + R_8 + R_{19}) & (R_1 + R_9 + R_{20}) & (R_2 + R_7 + R_{21}) \\ (R_{19} + R_{20} + R_{21}) & (R_2 + R_9 + R_{13}) & (R_3 + R_7 + R_{14}) & (R_1 + R_8 + R_{15}) \end{bmatrix} \tag{B12}$$

and from this matrix we see that the eigenvector for the A_g mode is

$$< A_g \mid = \frac{1}{\sqrt{12}} < 111\ \bar{1}\bar{1}1\ \bar{1}1\bar{1}\ 1\bar{1}\bar{1} \mid . \tag{B13}$$

This mode corresponds to the librations in which each molecule librates about their [111] directions in the same way. For the A_u mode the eigenvector is the same, but now molecules make displacements along their [111] directions instead of librations.

We now consider the projection operator for E_g modes

$$P(E_g) = \sum_{R \epsilon G_o(\Gamma)} \chi^*(E_g; R) T(\Gamma; R), \tag{B14}$$

and from the matrices $T(\Gamma; R)$ and $\chi^*(E_g; R)$ we get

$$P(E_g) = \begin{bmatrix} (R_1 + \epsilon R_2 + \epsilon^* R_3) & (R_7 + \epsilon R_{15} + \epsilon^* R_{20}) & (R_{13} + \epsilon R_8 + \epsilon^* R_{21}) & (R_{19} + \epsilon R_{14} + \epsilon^* R_9) \\ (R_7 + \epsilon^* R_8 + \epsilon R_9) & (R_1 + \epsilon R_{14} + \epsilon^* R_{21}) & (R_{19} + \epsilon R_2 + \epsilon^* R_{15}) & (R_{13} + \epsilon R_{20} + \epsilon^* R_3) \\ (R_{13} + \epsilon R_{14} + \epsilon^* R_{15}) & (R_{19} + \epsilon R_8 + \epsilon^* R_3) & (R_1 + \epsilon R_{20} + \epsilon^* R_9) & (R_7 + \epsilon R_2 + \epsilon^* R_{21}) \\ (R_{19} + \epsilon R_{20} + \epsilon^* R_{21}) & (R_{13} + \epsilon R_2 + \epsilon^* R_9) & (R_7 + \epsilon R_{14} + \epsilon^* R_3) & (R_1 + \epsilon R_8 + \epsilon^* R_{15}) \end{bmatrix}, \tag{B15}$$

where $\epsilon = e^{2\pi/3i}$ or we can take it as $(\epsilon + \epsilon^*)/2 = -\frac{1}{2}$. By applying this operator on the 12 orthonormal basis vectors $(1, \ldots, 0), \ldots, (0, \ldots, 1)$ we project three nonzero vectors of which only two are linearly independent. These, after normalization, have the following components:

$$< E_g^1 \mid = \frac{1}{\sqrt{24}} < \bar{1}\bar{1}2\ 112\ 1\bar{1}\bar{2}\ \bar{1}1\bar{2}\ \mid, \tag{B16}$$

$$< E_g^2 \mid = \frac{1}{\sqrt{8}} < 1\bar{1}0\ \bar{1}10\ \bar{1}\bar{1}0\ 110\ \mid . \tag{B17}$$

For the polarization vectors of the T_g modes, the procedure is a little complicated. First, we get three different projection operators $P_{\lambda,\lambda}(T_g)$ (λ=1–3) defined by

$$P_{\lambda,\lambda}(T_g)(q) = \left(\frac{f}{h}\right) \sum_{R \epsilon G_o(\Gamma)} \tau_{\lambda,\lambda}^{(T_g)}(\Gamma; R)^* T(\Gamma; R), \tag{B18}$$

where $\tau_{\lambda,\lambda}^{(T_g)}(\Gamma; R)$ is the $\lambda\lambda$th element of the matrix corresponding to the element R in the irreducible representation $\tau^{(T_g)}$. By applying this operator systematically on any 24 orthogonal vectors we can project out three orthogonal vectors. Each of these three vectors will trans-

form according to the λth row of the IR $\tau^{(T_g)}$. The partners of these vectors may be generated by applying to them the operator

$$P_{\mu,\lambda}(T_g) = \left(\frac{f}{h}\right) \sum_{R\epsilon G_o(\Gamma)} \tau^{(T_g)}_{\mu,\lambda}(\Gamma;R)^* T(\Gamma;R) \quad (\mu \neq \lambda). \tag{B19}$$

In this way, we can obtain three orthonormal sets corresponding to the three occurrences of T_g in $S(\Gamma)$. Here is the result:

$$< T^1_g\,|_1 = \frac{1}{\sqrt{24}} < \bar{1}\bar{1}2\ 112\ \bar{1}12\ 1\bar{1}2\ |, \tag{B20}$$

$$< T^1_g\,|_2 = \frac{1}{\sqrt{24}} < \bar{1}2\bar{1}\ \bar{1}21\ 121\ 12\bar{1}\ |, \tag{B21}$$

$$< T^1_g\,|_3 = \frac{1}{\sqrt{24}} < 2\bar{1}\bar{1}\ 2\bar{1}1\ 21\bar{1}\ 211\ |, \tag{B22}$$

$$< T^2_g\,|_1 = \frac{1}{\sqrt{8}} < 1\bar{1}0\ \bar{1}10\ 110\ \bar{1}\bar{1}0\ |, \tag{B23}$$

$$< T^2_g\,|_2 = \frac{1}{\sqrt{8}} < \bar{1}01\ \bar{1}0\bar{1}\ 10\bar{1}\ 101\ |, \tag{B24}$$

$$< T^2_g\,|_3 = \frac{1}{\sqrt{8}} < 01\bar{1}\ 011\ 0\bar{1}\bar{1}\ 0\bar{1}1\ |, \tag{B25}$$

$$< T^3_g\,|_1 = \frac{1}{\sqrt{12}} < 111\ \bar{1}\bar{1}1\ 1\bar{1}1\ \bar{1}11\ |, \tag{B26}$$

$$< T^3_g\,|_2 = \frac{1}{\sqrt{12}} < 111\ 11\bar{1}\ \bar{1}1\bar{1}\ \bar{1}11\ |, \tag{B27}$$

$$< T^3_g\,|_3 = \frac{1}{\sqrt{12}} < 111\ 11\bar{1}\ 1\bar{1}1\ 1\bar{1}\bar{1}\ |\,. \tag{B28}$$

Since A_g and E_g modes occur once, the symmetry-adapted vectors $|\,A_g>$ and $|\,E^1_g>, |\,E^2_g>$ given in Eqs. (B13), (B16), and (B17) can be taken to be eigenvectors of the dynamical matrix. For the T_g modes, eigenvectors are the linear combinations of the vectors $|\,T^i_g>_j$, i,j=1–3. Using these symmetry-adapted vectors, one can construct the diagonalizing matrix $\mathbf{Q}(\mathbf{\Gamma})$ which serves to transform $\mathbf{D}(\mathbf{\Gamma})$ into block diagonal form

$$\mathbf{Q}(\mathbf{\Gamma}) = \begin{bmatrix}
a & a & a & \bar{a} & \bar{a} & a & \bar{a} & a & \bar{a} & a & \bar{a} & \bar{a} \\
\bar{b} & \bar{b} & 2b & b & b & 2b & b & \bar{b} & 2\bar{b} & \bar{b} & b & 2\bar{b} \\
c & \bar{c} & 0 & \bar{c} & c & 0 & \bar{c} & \bar{c} & 0 & c & c & 0 \\
\bar{b} & \bar{b} & 2b & b & b & 2b & \bar{b} & b & 2b & b & \bar{b} & 2b \\
c & \bar{c} & 0 & \bar{c} & c & 0 & c & c & 0 & \bar{c} & \bar{c} & 0 \\
a & a & a & \bar{a} & \bar{a} & a & a & \bar{a} & a & \bar{a} & a & a \\
\bar{b} & 2b & \bar{b} & \bar{b} & 2b & b & b & 2b & b & b & 2b & \bar{b} \\
\bar{c} & 0 & c & \bar{c} & 0 & \bar{c} & c & 0 & \bar{c} & c & 0 & c \\
a & a & a & a & a & \bar{a} & \bar{a} & a & \bar{a} & \bar{a} & a & a \\
2b & \bar{b} & \bar{b} & 2b & \bar{b} & b & 2b & b & \bar{b} & 2b & b & b \\
0 & c & \bar{c} & 0 & c & c & 0 & \bar{c} & \bar{c} & 0 & \bar{c} & c \\
a & a & a & a & a & \bar{a} & a & \bar{a} & a & a & \bar{a} & \bar{a}
\end{bmatrix}, \tag{B29}$$

where

$$a = \frac{1}{2\sqrt{3}}, \quad b = \frac{1}{2\sqrt{6}}, \quad c = \frac{1}{2\sqrt{2}}. \tag{B30}$$

Before carrying out this block diagonalization, we need first to discuss the restrictions imposed by symmetry on the structure of $\mathbf{D}(\mathbf{\Gamma})$. For simplicity, we consider only the librational part of $\mathbf{D}(\mathbf{\Gamma})$ in Eq. (B1) and write it as

$$\mathbf{D}(\mathbf{\Gamma}) = \begin{bmatrix} D(11) & D(12) & D(13) & D(14) \\ D(21) & D(22) & D(23) & D(24) \\ D(31) & D(32) & D(33) & D(34) \\ D(41) & D(42) & D(43) & D(44) \end{bmatrix}, \tag{B31}$$

where $D(\mu\nu)$ are the 3×3 matrices with the matrix elements

$$D_{\alpha\beta}(\mu\nu) = \frac{1}{I}\sum_b \left(\frac{\partial^2 V_I}{\partial\theta_\alpha(o,\mu)\partial\theta_\beta(b,\nu)}\right)_o. \tag{B32}$$

Now it is possible to discover interrelations among the elements of $\mathbf{D}(\mathbf{\Gamma})$ using purely symmetry arguments. The simplifications sought for arise basically from the commutation relation $[\mathbf{D}(\mathbf{\Gamma}), T(\Gamma;R_i)] = 0$ for any operation R_i of the point group T_h. Actually, from these commutation relations one can show that

$$R_i D(\mu\nu) R_i^+ = D(\mu'\nu'), \tag{B33}$$

where $\mu \to \mu'$ and $\nu \to \nu'$ under the operation R_i.

With use of this equation simplifications of the dynamical matrix is a straightforward matter and thus we directly give the final form of the dynamical matrix which has eight independent parameters and is given by

$$\mathbf{D}(\mathbf{\Gamma}) = \begin{bmatrix}
\alpha & \beta & \beta & k & \gamma & -\delta & \epsilon & \lambda & \gamma & h & \delta & -\lambda \\
\beta & \alpha & \beta & \gamma & \epsilon & \lambda & -\lambda & h & \delta & -\delta & k & \gamma \\
\beta & \beta & \alpha & \delta & -\lambda & h & \gamma & -\delta & k & \lambda & \gamma & \epsilon \\
k & \gamma & \delta & \alpha & \beta & -\beta & h & \delta & \lambda & \epsilon & \lambda & -\gamma \\
\gamma & \epsilon & -\lambda & \beta & \alpha & -\beta & -\delta & k & -\gamma & -\lambda & h & -\delta \\
-\delta & \lambda & h & -\beta & -\beta & \alpha & -\lambda & -\gamma & \epsilon & -\gamma & \delta & k \\
\epsilon & -\lambda & \gamma & h & -\delta & -\lambda & \alpha & -\beta & \beta & k & -\gamma & -\delta \\
\lambda & h & -\delta & \delta & k & -\gamma & -\beta & \alpha & -\beta & -\gamma & \epsilon & -\lambda \\
\gamma & \delta & k & \lambda & -\gamma & \epsilon & \beta & -\beta & \alpha & \delta & \lambda & h \\
h & -\delta & \lambda & \epsilon & -\lambda & -\gamma & k & -\gamma & \delta & \alpha & -\beta & -\beta \\
\delta & k & \gamma & \lambda & h & \delta & -\gamma & \epsilon & \lambda & -\beta & \alpha & \beta \\
-\lambda & \gamma & \epsilon & -\gamma & -\delta & k & -\delta & -\lambda & h & -\beta & \beta & \alpha
\end{bmatrix} \tag{B34}$$

For translational modes the number of independent parameters in $\mathbf{D}(\mathbf{\Gamma})$ can be reduced further. Since we have three acoustic modes in which the whole crystal moves together, the eigenvectors $<$ 100 100 100 100 $|$, $<$ 010 010 010 010 $|$, $<$ 001 001 001 001 $|$ must have zero eigenvalues. Thus we have the following constraints:

$$\alpha + k + \epsilon + h = 0, \tag{B35}$$

$$\beta+\gamma+\lambda+\delta=0, \tag{B36}$$

$$\beta+\gamma-\lambda-\delta=0. \tag{B37}$$

The form deduced above for $\mathbf{D}(\Gamma)$ is the most general one consistent with crystal symmetry. We observe that whereas by considering the Hermitian property alone there will be 72 independent elements in $\mathbf{D}(\Gamma)$, systematic use of group theoretical arguments shows that there are only eight independent elements for libron and five for phonon modes.

What remains now is to bring $\mathbf{D}(\Gamma)$ into the block-diagonal form $\mathcal{D}(\Gamma)$. This is done by performing the transformation

$$\mathcal{D}(\Gamma)=\mathbf{Q}(\Gamma)\mathbf{D}(\Gamma)\mathbf{Q}(\Gamma)^{+}. \tag{B38}$$

Since $\mathbf{D}(\Gamma)$ and $\mathbf{Q}(\Gamma)$ are known, evaluation of Eq. (B38) is a straightforward matter (with use of the computer program REDUCE). The resulting block-diagonal matrix $\mathcal{D}(\Gamma)$ has the form

$$\mathcal{D}(\Gamma)=\begin{bmatrix} E(A_g) & & & & & \\ & E(E_g) & & & & \\ & & E(E_g) & & & \\ & & & E(T_g) & & \\ & & & & E(T_g) & \\ & & & & & E(T_g) \end{bmatrix}, \tag{B39}$$

where the 1×1 matrices $E(A_g)$, $E(E_g)$ are

$$E(A_g)=\alpha+h-\epsilon-k+2(\beta+\lambda-\delta-\gamma), \tag{B40}$$

$$E(E_g)=\alpha+h-\epsilon-k-(\beta+\lambda-\delta-\gamma), \tag{B41}$$

and 3×3 symmetric matrix $E(T_g)$ is

$$E(T_g)=\begin{bmatrix} \frac{3(\alpha-\beta)+2(k+\epsilon)-5\gamma+\delta+h-\lambda}{3} & -\frac{2(\delta+\lambda)-k+\epsilon}{\sqrt{3}} & \frac{2[\delta-k-\lambda-\epsilon-2(h+\gamma)]}{3\sqrt{2}} \\ -\frac{2(\delta+\lambda)-k+\epsilon}{\sqrt{3}} & \alpha+\gamma+\lambda-\beta-\delta-h & -\frac{2[\delta+k+\lambda-\epsilon]}{\sqrt{6}} \\ \frac{2[\delta-k-\lambda-\epsilon-2(h+\gamma)]}{3\sqrt{2}} & -\frac{2[\delta+k+\lambda-\epsilon]}{\sqrt{6}} & \frac{3(\alpha+2\beta)+2(\delta+\gamma-\lambda)-h+k+\epsilon}{3} \end{bmatrix}. \tag{B42}$$

For phonon modes these expressions become much simpler due to the constraints given in Eqs. (B35)–(B37).

[1] P. A. Heiney, J. E. Fischer, A. R. McGhie, W. J. Romanow, A. M. Denenstein, J. P. McCauley, Jr., and A. B. Smith III, Phys. Rev. Lett. **66**, 2911 (1991).

[2] G. A. Samara, J. E. Schirber, B. Morosin, L. V. Hansen, D. Loy, and A. P. Sylwester, Phys. Rev. Lett. **67**, 3136 (1991); G. Kriza, J.-C. Ameline, D. Jerome, A. Dworkin, H. Szwarc, C. Fabre, D. Schuta, A. Rassat, and P. Bernier, J. Phys. I (France) **1**, 1361 (1991).

[3] R. M. Fleming, T. Siegrist, P. M. March, B. Hessen, A. R. Kortan, D. W. Murphy, R. C. Haddon, R. Tycko, G. Dabbagh, A. M. Mujsce, M. L. Kaplan, and S. M. Zahurak, *Materials Research Society Symposium Proceedings* (Materials Research Society, Pittsburgh, 1991), Vol. 206, p. 691.

[4] R. Tycho, G. Dabbagh, R. M. Fleming, R. C. Haddon, A. V. Makhija, and S. M. Zahurak, Phys. Rev. Lett. **67**, 1886 (1991).

[5] A. B. Harris and R. Sachidanandam, Phys. Rev. B **46**, 4944 (1992).

[6] R. Sachidanandam and A. B. Harris, Phys. Rev. Lett. **67**, 1467 (1991). See also Ref. 27.

[7] P. A. Heiney, J. E. Fischer, A. R. McGhie, W. J. Romanow, A. M. Denenstein, J. P. McCauley, A. M. Smith III, and D. E. Cox, Phys. Rev. Lett. **67**, 1468 (1991).

[8] W. I. F. David, R. M. Ibberson, T. J. S. Dennis, J. P. Hare, and K. Prassides, Europhys. Lett. (to be published).

[9] G. Van Tendeloo, C. Van Heurck, J. Van Landuyt, S. Amelinckx, M. A. Verheijen, P. H. M. van Loosdrecht, and G. Meijer (unpublished).

[10] J. P. Lu, X.-P. Li, and R. M. Martin, Phys. Rev. Lett. **68**, 1551 (1992).

[11] M. Sprik, A. Cheng, and M. L. Klein, J. Phys. Chem. **96**, 2027 (1992).

[12] X.-P. Li, J. P. Lu, and R. M. Martin (unpublished).

[13] G. Venkataraman and V. C. Sahni, Rev. Mod. Phys. **42**, 409 (1970).

[14] For instance, the minimum frequency of intramolecular vibrations is observed to be about 270 cm^{-1}. See R. L. Cappelletti, J. R. D. Copley, W. A. Kamitakahara, Fang Li, J. S. Lannin, and D. Ramage, Phys. Rev. Lett. **66**, 3261 (1991). As we shall see this frequency is much higher than that (~ 50 cm^{-1}) for intermolecular vibrations.

[15] O. Schnepp and A. Ron, Discuss. Faraday Soc. **48**, 26 (1969).

[16] S. H. Walmsley and J. A. Pople, Mol. Phys. **8**, 345 (1964).

[17] J. Van Kranendonk, *Solid Hydrogen* (Plenum, New York, 1982).

[18] I. F. Silvera, Rev. Mod. Phys. **52**, 393 (1980).

[19] A. J. Berlinsky and C. F. Coll III, Phys. Rev. B **5**, 1587 (1971).

[20] F. G. Mertens and W. Biem, Z. Phys. **250**, 273 (1972).

[21] A. Bickermann, W. Biem, and F. G. Mertens, Z. Phys. **267**, 31 (1974).

[22] A. B. Harris and A. J. Berlinsky, Phys. Rev. B **16**, 3791 (1977).

[23] H. Goldstein, *Classical Mechanics* (Addison-Wesley, Reading, MA, 1953).

[24] S. Califona, *Vibrational Spectroscopy of Molecular Liquids and Solids* (Plenum, New York, 1980), p. 221.

[25] N. Neto, R. Righini, S. Califano, and S. H. Walmsley, Chem. Phys. **29**, 167 (1978).

[26] A. Cheng and M. L. Klein, J. Phys. Chem. **95**, 6750 (1991).

[27] W. I. F. David, R. M. Ibberson, J. C. Matthewman, K. Prassides, T. J. S. Dennis, J. P. Hare, H. W. Kroto, R. Taylor, and D. R. M. Walton, Nature (London) **353**, 147 (1991).

[28] A. A. Maradudin and S. H. Vosko, Rev. Mod. Phys. **40**, 1

(1968).
[29]G. F. Koster, in *Solid State Physics*, edited by H. Ehrenreich, F. Seitz, and D. Turnbull (Academic, New York, 1957), Vol. 5, p. 173.
[30]O. V. Kovalev, *Irreducible Representations of the Space Groups* (Gordon and Breach, New York, 1965).
[31]D. A. Neumann, J. R. D. Copley, W. A. Kamitakahara, J. J. Rush, R. L. Capelletti, N. Coustel, J. P. McCauley, Jr., J. E. Fischer, A. B. Smith III, K. M. Creegan, and D. M. Cox (unpublished).
[32]O. Schnepp, J. Chem. Phys. **46**, 3983 (1967).
[33]R. Jochemsen, A. J. Berlinsky, F. Verspaandonk, and Isaac F. Silvera, J. Low Temp. Phys. **32**, 185 (1978).
[34]C.F. Coll III, A. B. Harris, and A. J. Berlinsky, Phys. Rev. Lett. **25**, 858 (1970).
[35]A. D. Buckingham and G. C. Tabisz, Mol. Phys. **36**, 583 (1978).
[36]P. H. M. van Loosdrecht, P. J. M. van Bentum, and G. Meijer, Phys. Rev. Lett. **68**, 1176 (1992).
[37]P. A. Heiney and G. B. M. Vaughan (private communication).